



Designing an Optimal LSST Deep Drilling Program for Cosmology with Type Ia Supernovae

Philippe Gris¹, Nicolas Regnault², Humna Awan³, Isobel Hook⁴, Saurabh W. Jha⁵, Michelle Lochner^{6,7}, Bruno Sanchez⁸, Dan Scolnic⁸, Mark Sullivan⁹, Peter Yoachim¹⁰, and The LSST Dark Energy Science Collaboration

¹ Laboratoire de Physique de Clermont, IN2P3/CNRS, F-63000 Clermont-Ferrand, France

² Laboratoire de Physique Nucléaire et des Hautes Energies, IN2P3/CNRS, France

³ Leinweber Center for Theoretical Physics, Department of Physics, University of Michigan, Ann Arbor, MI 48109, USA

⁴ Physics Department, Lancaster University, Lancaster LA1 4YB, UK

⁵ Department of Physics and Astronomy, Rutgers, The State University of New Jersey, Piscataway, NJ 08854, USA

⁶ Department of Physics and Astronomy, University of the Western Cape, Bellville, Cape Town 7535, South Africa

⁷ South African Radio Astronomy Observatory (SARAO), The Park, Park Road, Pinelands, Cape Town 7405, South Africa

⁸ Department of Physics, Duke University, Durham, NC 27708, USA

⁹ School of Physics and Astronomy, University of Southampton, Southampton, SO17 1BJ, UK

¹⁰ University of Washington, 4333 Brooklyn Avenue NE, Seattle, WA 98105, USA

Received 2022 June 2; revised 2022 October 5; accepted 2022 October 26; published 2023 January 11

Abstract

The Vera C. Rubin Observatory's Legacy Survey of Space and Time (LSST) is forecast to collect a large sample of Type Ia supernovae (SNe Ia) expected to be instrumental in unveiling the nature of dark energy. The feat, however, requires accurately measuring the two components of the Hubble diagram, distance modulus and redshift. Distance is estimated from SN Ia parameters extracted from light-curve fits, where the average quality of light curves is primarily driven by survey parameters. An optimal observing strategy is thus critical for measuring cosmological parameters with high accuracy. We present in this paper a three-stage analysis to assess the impact of the deep drilling (DD) strategy parameters on three critical aspects of the survey: redshift completeness, the number of well-measured SNe Ia, and cosmological measurements. We demonstrate that the current DD survey plans (internal LSST simulations) are characterized by a low completeness ($z \sim 0.55\text{--}0.65$), and irregular and low cadences (several days), which dramatically decrease the size of the well-measured SN Ia sample. We propose a method providing the number of visits required to reach higher redshifts. We use the results to design a set of optimized DD surveys for SN Ia cosmology taking full advantage of spectroscopic resources for host galaxy redshift measurements. The most accurate cosmological measurements are achieved with deep rolling surveys characterized by a high cadence (1 day), a rolling strategy (at least two seasons of observation per field), and ultradeep ($z \gtrsim 0.8$) and deep ($z \gtrsim 0.6$) fields. A deterministic scheduler including a gap recovery mechanism is critical to achieving a high-quality DD survey.

Unified Astronomy Thesaurus concepts: [Cosmological parameters \(339\)](#)

1. Introduction

Type Ia supernovae (SNe Ia) are transient astronomical events resulting from a powerful and luminous explosion of a white dwarf. They display a characteristic brightness evolution, with a luminosity peak about 15 days after explosion, and a slow decrease lasting up to several months. SNe Ia can be used as standardizable candles to determine cosmological distances. Use of the Hubble diagram of SNe Ia is the most statistically efficient approach to constraining the dark energy equation of state (Betoule et al. 2014; Scolnic et al. 2018a).

The Vera C. Rubin Observatory (VRO) Legacy Survey of Space and Time (LSST; Ivezić et al. 2019) will discover some millions of SNe during 10 years of operations (Abell et al. 2009). This number is quite impressive but in a sense misleading. If the survey is not optimized, a large fraction of these SNe Ia will be useless for cosmological measurements because of large luminosity distance errors. An optimized

survey aims at *observing a large sample* (a few thousands spanning a broad range of redshifts to be limited by systematic uncertainties) of *well-measured* SNe Ia with distance measurements accurate to better than $\sim 5\%$ at higher z . The criteria defining well-measured SNe Ia are to be found in Section 4.

The 10-year LSST will image billions of objects in six bands. Eighty to ninety percent of the observing time will be dedicated to the wide–fast–deep (WFD) primary survey, which will cover half of the sky ($\sim 18,000 \text{ deg}^2$) at a universal¹¹ cadence. The cadence is defined as the median internight gap in any filter. *High* cadences are characterized by *small* internight gaps. The remaining observing time will be shared among other programs (minisurveys) including intensive scanning of a set of deep drilling fields (DDFs). It is not clear yet what fraction of SNe Ia observed in the WFD and deep drilling (DD) surveys will be confirmed from spectral features. But spectroscopically confirmed SNe Ia will certainly represent a small part of the SN Ia sample. Accurate SN Ia parameters will thus be estimated from well-measured light curves characterized by a sampling of several days and high signal-to-noise ratios per band (S/N^b).



Original content from this work may be used under the terms of the [Creative Commons Attribution 4.0 licence](#). Any further distribution of this work must maintain attribution to the author(s) and the title of the work, journal citation and DOI.

¹¹ Fields are observed with a similar cadence and pattern.

Obtaining these high-quality light curves is therefore a key design point of the SN survey: the average quality of the light curves depends primarily on the observing strategy.

In a recent paper (Lochner et al. 2022), the LSST Dark Energy Science Collaboration (DESC) has presented an analysis from the WFD survey observing strategies simulated by the LSST project.¹² The conclusion is that an unprecedented number of well-measured SNe Ia will be observed in the WFD survey (between 120,000 and 170,000) up to redshifts $z \sim 0.3$. The DD minisurvey of LSST is critical for observing a sample of high-redshift and well-measured SNe Ia so as to achieve Stage IV dark energy goals (Albrecht et al. 2006). Optimizing the LSST DD survey so as to collect a large sample of well-measured SNe Ia up to high redshift fulfilling this requirement while taking into account survey constraints (the time budget) is one of the main purposes of this paper. The work presented is a further step of a process started more than five years ago (Scolnic et al. 2018b; Lochner et al. 2021).

There are critical LSST survey parameters, such as the scanning strategy, cadence, and filter allocation, that are not defined yet. Ongoing efforts are being made to define the requirements to accomplish the four primary science objectives of the VRO: characterization of dark energy and dark matter, inventory of the solar system, transient optical sky exploration, and mapping of the Milky Way. As of 2020, the Survey Cadence Optimization Committee (SCOC; Bianco et al. 2021) has been charged to make specific recommendations for the survey parameter choices for LSST (the initial survey strategy for 10 years) based on input from the science community. The studies presented in this paper are part of the global effort aiming to define the optimal strategy parameters to accomplish the scientific objectives of the VRO.

This paper deals with the interplay between the DD strategy and the SN Ia sample collected by the survey. We perform a detailed study of the impact of the strategy parameters (the number of fields to observe, the number of seasons, the season lengths, and the number of visits¹³ per night and per field) on the SN Ia sample quality to assess whether observing SNe up to $z \simeq 0.8\text{--}0.9$ is achievable given design constraints, including in particular the number of visits allotted to DDFs. This article is subdivided into eight sections. The requirements for SNe and the design constraints of the DD program are presented in Sections 2 and 3. The metrics used to assess observing strategies are defined in Section 4 and used in a detailed analysis of LSST simulations in Section 5. One of the conclusions of this analysis is that the samples collected with the proposed strategies could be too shallow and we propose in Section 6 a method aiming at increasing the depth of the DD survey. We use the results of this method to design optimized DD surveys that would achieve the goal of observing well-measured SNe Ia up to higher redshifts (Sections 7–9).

2. Requirements for SNe

SNe Ia have been demonstrated as precise and reliable distance indicators over the past decade (Scolnic et al. 2018a; Abbott et al. 2019; Brout et al. 2022). Distances are derived from SN Ia parameters that are inferred from photometric light curves. The accuracy of the distance estimation reflects the

precision of the photometric measurements. We discuss in the following subsection (Section 2.1) the light-curve quality criteria that are required to obtain accurate distance measurements.

SN surveys are magnitude-limited and gather samples affected by a selection effect called the Malmquist bias (Malmquist 1922; Teerikorpi 2015, and references therein): brighter SNe Ia are preferentially discovered at the faint limits of the survey. This redshift-varying bias has an impact on the measurement of cosmological parameters and is to be taken into account in the design of the survey (Section 2.2).

2.1. Distance Measurement and Well-measured SNe

The diversity of SN Ia light curves is usually parameterized by three parameters: the amplitude (brightness), the color, and the light-curve width (shape). The Tripp estimator (Tripp & Branch 1999 and references therein) uses the B -band absolute magnitude, the $(B - V)$ color, and the rate of decline during the first 15 days after the maximum, Δm_{15} , to standardize the SN Ia brightness and estimate the distance. In the SALT2 light-curve model (Guy et al. 2007, 2010), the distance modulus, μ , is defined for each SN Ia by

$$\mu = m_B + \alpha x_1 - \beta c - M \quad (1)$$

where $m_B = -2.5 \log_{10}(x_0) + 10.635$ (where x_0 is the overall flux normalization), x_1 describes the width of the light curve, and c is equal to the color offset (with respect to the average) at the date of peak brightness in the B band, $c = (B - V)_{\text{MAX}} - \langle B - V \rangle$. For each SN Ia, the m_B , x_1 , and c parameters are estimated from a fit of the SN Ia model to the measurements of a multicolor light curve. The parameters α , β , and M are global parameters estimated from the data. M is the absolute magnitude in the rest-frame B band for a median SN Ia with $(x_1, c) = (0.0, 0.0)$. The parameters α and β are global nuisance parameters quantifying the correlation of brightness with x_1 and c , respectively. The three parameters α , β , and M are fitted along with the cosmological parameters by minimizing the distance scatter. Accurate luminosity distances (i.e., accurate estimations of the SN Ia standardization parameters m_B , x_1 , and c) are thus critical to constraining cosmological parameters with better precision.

The relative contribution of the SN Ia parameter errors to the uncertainty on the distance modulus σ_μ is driven by the values of the nuisance parameters α and β . Recent measurements (Scolnic et al. 2018a; Abbott et al. 2019) confirm that β is larger than 3, that α is around 0.16, and that measured values of x_1 and c lie in limited ranges, $[-3.0, 3.0]$ and $[-0.3, 0.3]$, respectively. The consequence is that the color term $\beta\sigma_c$ is dominant in the σ_μ budget as illustrated in Figure 1. The dispersion of Hubble residuals due to the intrinsic scatter of the standardized SN Ia brightness (Brout & Scolnic 2021) is of 0.12–0.14 mag (Betoule et al. 2014; Scolnic et al. 2018a). Measurement uncertainties on the color above ~ 0.04 will thus make a significant contribution to the distance modulus errors. The requirement $\sigma_c \lesssim 0.04$ is one of the main criteria (see Section 4) that designate a *well-measured* SN Ia. It implicitly defines a redshift limit z_{lim} (Figure 1) above which SN Ia light-curve measurements lead

¹² <https://community.lsst.org/t/community-survey-strategy-highlights>

¹³ A visit is a single observation of an LSST field comprised of two 15 s exposures that are immediately combined or one 30 s exposure.

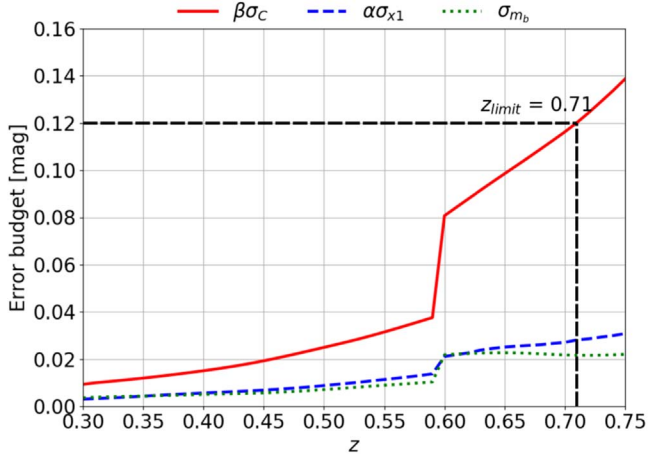


Figure 1. Contributions to the uncertainty of the distance modulus σ_μ as a function of the redshift. Three components are represented: the color component ($\beta\sigma_c$), the stretch component ($\alpha\sigma_{x_1}$), and the amplitude component (σ_{m_b}). The color component starts to contribute significantly to the distance uncertainty above $\beta\sigma_c \sim 0.12$ (or equivalently $\sigma_c \sim 0.04$). This threshold corresponds to the redshift limit value (here 0.71) for the observation of well-measured SNe Ia. These results are obtained from a full simulation of SN Ia light curves (regular cadence of 1 day). The SN Ia parameters are estimated from a SALT2 fit. The r -band measurements are not taken into account for $z \gtrsim 0.6$ (sharp slopes) because of large model uncertainties (see Section 4 for more details).

to error budget-limited distance measurements:

$$\sigma_c \leqslant 0.04 \implies z_{\text{lim}}. \quad (2)$$

The uncertainty on m_b , x_1 , and c is driven by the quality of the collected light curves, which is defined by the sampling frequency of the measurements (the cadence of observation) and by the light-curve points' uncertainties (the observing conditions). The σ_c estimation is a function of S/N^b , defined by

$$S/N^b = \sqrt{\sum_{i=1}^{n^b} \left(\frac{f_i^b}{\sigma_i^b} \right)^2} \quad (3)$$

where f^b and σ^b denote the fluxes and flux uncertainties. The summation runs over the number of light-curve points. Requiring $\sigma_c \leqslant 0.04$ is equivalent to requiring a minimal S/N^b (Figure 2) and the link between z_{lim} and S/N^b may be written as

$$\wedge(S/N^b \geq S/N_{\min}^b) \implies \sigma_c \leq 0.04 \implies z_{\text{lim}} \quad (4)$$

where the logical symbol \wedge means that the requirement $S/N^b \geq S/N_{\min}^b$ is to be fulfilled for all considered bands.

2.2. Redshift Completeness

As with all other flux-limited surveys, a larger fraction of bright SNe Ia of the DD survey will systematically be observed at high redshift. SNe Ia observed at the fainter ends of the luminosity distribution are characterized by a mean intrinsic peak brightness higher than the mean of the whole sample. This bias increases with redshift and affects the distance estimation: the effective luminosity is biased toward brighter values. This leads to shorter-distance measurements.

It is possible to estimate distance biases using simulation of unobserved events (Kessler et al. 2013; Scolnic & Kessler 2016). Recent cosmological analysis (Scolnic et al. 2018a; Riess et al. 2019) has used the BEAMS with Bias

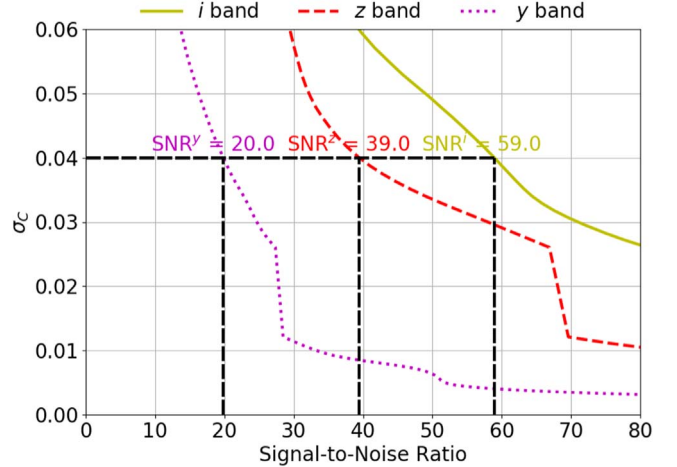


Figure 2. Color uncertainty as a function of S/N^b . Requiring $\sigma_c \leq 0.04$ is equivalent to applying the following selections: $S/N^i \geq 59$, $S/N^z \geq 39$, and $S/N^y \geq 20$. These results are obtained from a full simulation of SN Ia light curves for an intrinsically faint SN Ia (i.e., with $(x_1, c) = (-2.0, 0.2)$) and a regular cadence of 1 day. The SN Ia parameters are estimated from a SALT2 fit. The r -band measurements are not taken into account for $z \gtrsim 0.6$ (sharp slopes in S/N^z and S/N^y around 67 and 27, respectively) because of large model uncertainties (see Section 4 for more details).

Corrections framework (Kessler & Scolnic 2017), which includes corrections dependent on α and β in the SN Ia cosmology likelihood. With this method, distance bias corrections have a clear impact on the cosmological measurements (the shift of the dark energy parameter w decreases from 7% to 1%) but the systematic uncertainty related to the selection bias still accounts for more than 20% of the total systematic error budget (Scolnic et al. 2018a). An incomplete high-redshift sample is thus affected by a systematic uncertainty (due to selection bias) that could be dominant in high-redshift, magnitude-limited surveys like the LSST DD survey. More importantly, the Malmquist bias leads to a decrease in the number of SNe Ia for $z \geq z_{\text{complete}}$, where z_{complete} is the redshift completeness due to the Malmquist bias. It is the redshift above which intrinsically faint SNe Ia cannot be observed (the method to estimate z_{complete} is explained in Section 4). The fraction of higher-redshift SNe Ia decreases with z_{complete} . The redshift completeness value thus has an impact on SN Ia cosmology since accurate cosmological measurements with a Hubble diagram heavily rely on the distribution of the number of well-measured SNe Ia as a function of the redshift, $N(z)$. We will quantify this impact in Section 7.

There are two ways to optimize the cosmological constraints from SNe Ia in a limited time budget survey. In the first scenario, the total number of well-measured SNe Ia can be maximized by observing all the DDFs for 10 yr with a low universal cadence (i.e., the same z_{complete}). The second approach consists in maximizing the redshift completeness by observing the DDFs at a higher cadence but in a limited number of years. We will study in Section 7 these two scenarios, (high N_{SN} , low z_{complete}) and (low N_{SN} , high z_{complete}).

3. Observing Strategy Constraints

The design parameters are the number of fields to be observed, the number of seasons of observation and the season

Table 1
Location of the DDFs Considered in This Study

Field Name	Central R.A. (J2000)	Central Decl. (J2000)
ELAIS-S1	00:37:48	-44:01:30
XMM-LSS	02:22:18	-04:49:00
CDF-S	03:31:55	-28:07:00
COSMOS	10:00:26	+02:14:01
ADF-A	04:51:00	-52:55:00
ADF-B	04:35:00	-54:40:00

Note. The AKARI Deep Fields (ADF-A and ADF-B) are examples of southern fields in the Euclid/Roman area simulated in the LSST observing strategy.

length, the cadence of observation, the filter allocation, and the total observing time budget.

The VRO defined in 2012¹⁴ four extragalactic DDFs: COSMOS, ELAIS-S1, XMM-LSS, and CDF-S (Table 1). More recently, DESC has supported the LSST DDF coverage of the southern deep-field area (Lochner et al. 2021) to ensure contemporaneous observations with Euclid (Laureijs et al. 2011; Amendola et al. 2013) and the Roman Space Telescope (Spergel et al. 2015) at the beginning and at the midterm of LSST, respectively.

The number of observed SNe is proportional to the number of seasons of observation and to the season duration (Perrett et al. 2012). The season length of a field is equal to the period of observability,¹⁵ which depends on the field’s location with respect to the VRO. It is driven by the nightly observable time, which can be converted to the number of visits per observing night (N_{visits}). The estimation of the season length as a function of the total number of visits for the fields defined in Table 1 (Figure 3) suggests a decrease from 275–200 days to 150–100 days when N_{visits} increases from 1 to 400. Season lengths of at least 6 months are required to collect at least 80% of the SNe Ia of the northernmost fields. Maximizing season length is particularly important in the DDFs because of time dilation. High- z SN Ia light curves last longer than low- z ones. SNe Ia collected at the beginning and at the end of the season are characterized by poorly reconstructed light curves leading to inaccurate distance measurements. Time dilation effects may be quantified as an effective season length decreasing with z .

A regular cadence of observation (~ 3 days maximum) is required to collect well-measured light curves. Large gaps (> 10 days) between visits degrade the measurements of luminosity distances, and potentially result in rejection of large sets of light curves of poor quality. It could be critical to have a scheduler including a gap recovery mechanism to collect a large sample of well-measured light curves leading to accurate cosmological measurements. We propose in Section 9 a set of methods to recover from gap effects.

Measuring cosmological parameters with high accuracy requires observing SNe Ia over a wide redshift range $z \in [0.01, 1.1]$. Five filters of the VRO thus have to be used— g , r , i , z , and y —with the number of visits per band and per night depending on the redshift completeness of the survey (Section 6).

¹⁴ <http://ls.st/bki>

¹⁵ An astronomical target is said to be observable if it is visible (for the VRO, having $20^\circ \leqslant \text{altitude} \leqslant 86.5^\circ$ and $\text{airmass} \leqslant 1.5$) for a minimal amount of time.

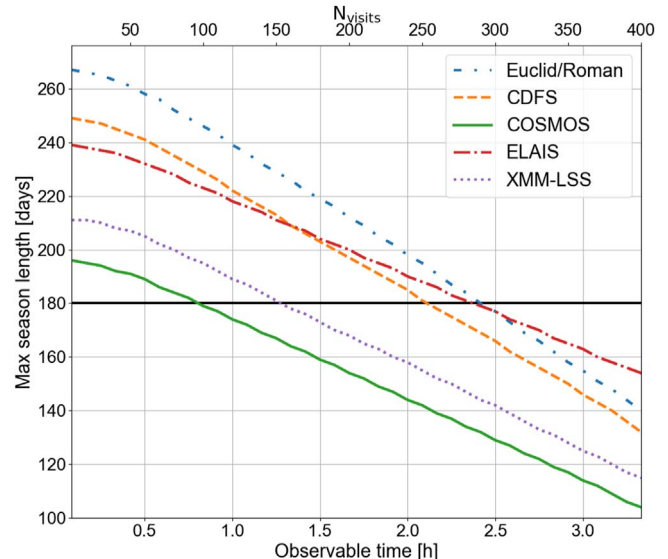


Figure 3. Maximal season length as a function of the nightly observable time (in hours) (lower x -axis) or the number of visits (upper x -axis) per observing night. Fields are observable if the following requirements are met: $20^\circ \leqslant \text{altitude} \leqslant 86.5^\circ$, and $\text{airmass} \leqslant 1.5$. This plot is made using scripts and tools of the LSST scheduler. The black line corresponds to a season length of 180 days.

It is expected that 5%–15% of the total number of LSST visits will be allotted to the DD program and shared among science topics of interest to DD observations (such as active galactic nuclei, SNe, and photo- z training). The DD time budget is defined as the fraction of observing time allotted to DDFs during the survey. For the sake of simplicity we will assume that the exposure time of observation does not change during the survey. In that case the DD time budget is defined by

$$\text{DD}_{\text{budget}} = N_{\text{visits}}^{\text{DD}} / (N_{\text{visits}}^{\text{DD}} + N_{\text{visits}}^{\text{non-DD}}) \quad (5)$$

where $N_{\text{visits}}^{\text{DD}}$ is the total number of visits (for the 10 years of VRO operation) allocated to DDFs and is defined by

$$N_{\text{visits}}^{\text{DD}} = \sum_{i=1}^{N_{\text{fields}}} \sum_{j=1}^{N_{\text{season}}^i} N_{\text{visits}, \text{night}}^{ij} \times \text{seaslen}^{ij} / \text{cad}^{ij} \quad (6)$$

where N_{fields} is the number of DDFs, N_{season} is the number of seasons of observation per field, seaslen is the season length (in days), cad is the cadence of observation, and $N_{\text{visits}, \text{night}}^{ij}$ is the total number of visits per observing night per field per season. The total number of visits corresponding to all fields but the DDFs, $N_{\text{visits}}^{\text{non-DD}}$, is estimated from a sample of LSST simulations and set to 2,122,176 (10 yr of survey). The DD time budget is fairly strongly dependent on the number of visits per observing night and on the season length (Figure 4): the total number of visits is multiplied by 5 if the budget increases from 3% to 15%.

4. Metrics to Assess Observing Strategies

The metrics used to assess observing strategies are estimated from a full simulation and fit of light curves. We use SNCosmo¹⁶ (Barbary et al. 2016) (version 2.1.0 released in 2020 February), a Python library synthesizing SN spectra and photometry from SN models. It includes a lot of built-in SN

¹⁶ <https://sncosmo.readthedocs.io/en/latest/index.html>

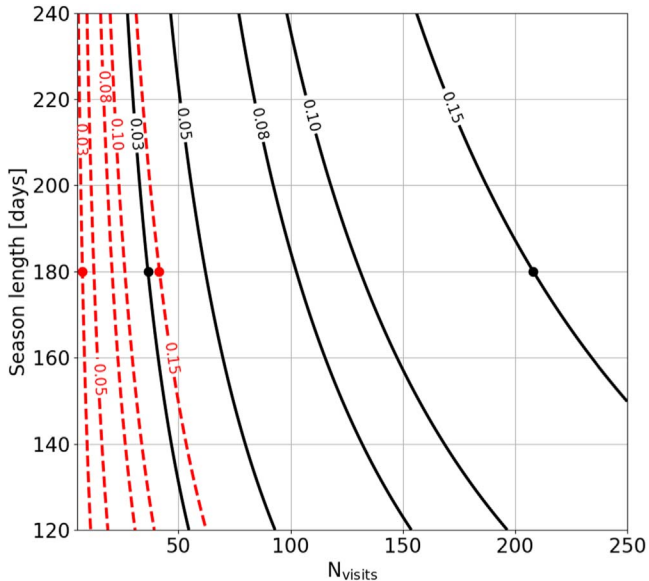


Figure 4. DD time budget contours in the plane (N_{visits} , season length) for a configuration of five fields with 2 (black) or 10 (red) observing seasons per field and a cadence of 1 day. The number of visits dramatically decreases with the number of seasons of observation when the time budget is limited. For a typical season length of 180 days and a time budget extending from 3% (minimal) to 15% (maximal), the number of visits ranges from 7 to 42 for 10 seasons (dashed red lines). Decreasing the number of seasons to 2 leads to an increase in the possible number of visits, from 36 to 208 (solid black lines).

models (SALT2, SALT3, MLCS2k2, Hsiao, Nugent, and Whalen models, as well as models from SNANA), as well as a variety of built-in bandpasses and magnitude systems. It includes functions for fitting and sampling SN model parameters given photometric light-curve data. We use the SALT2 model (SALT2.4; Betoule et al. 2014 and references therein), where an SN Ia is described by five parameters: x_0 , x_1 , c , z , and T_0 , the time of maximum luminosity. The SALT2 model has been extensively tested and used in cosmology analyses in the last decade. A flat Λ CDM model is used to estimate cosmological distances, with $H_0 = 70 \text{ km s}^{-1}$, $\Omega_m = 0.3$, and $\Omega_\Lambda = 0.7$.

The SALT3 model (Kenworthy et al. 2021) was implemented in SNCosmo (version 2.5.0) in 2021 April. The work presented in this paper had made significant progress by that time and including this new model would have led to delays that we cannot afford in the context of these studies (the decision of the SCOC should be made by the end of 2022). Nonetheless we estimate the impact of the SALT3 model on a key result of the paper (Section 6) and we observe a slight improvement with respect to the ubiquitous SALT2 model.

In SALT2, model uncertainties of the g - and r -band (rest-frame UV) light-curve fluxes are large (Guy et al. 2007), and g and r observations with relative errors of the model larger than 5% are not considered in this study. This requirement implies that the list of filters useful for measuring photometric light curves (in the observer frame) is redshift-dependent (Table 2).

Following the requirements for SNe (Section 2), we rely on two metrics to assess observing strategies: the redshift completeness z_{complete} , and the number of well-measured SNe Ia, $N_{\text{SN}}^{z \leq z_{\text{complete}}}$. A well-measured SN Ia is defined by the following tight selection criteria:

Table 2
List of Filters Useful for Measuring Photometric Light Curves (in Observer Frame) as a Function of Redshift

z	[0.01, 0.1]	[0.1, 0.35]	[0.35, 0.65]	[0.65, 1.1]
bands	<i>gri</i>	<i>griz</i>	<i>rizy</i>	<i>izy</i>

- only light-curve points with $S/N \geq 1$ are considered;
 - at least 4 epochs before the maximum luminosity and 10 epochs after the maximum luminosity are required;
 - at least one point with a phase¹⁷ lower than -10° and one point with a phase higher than 20° are required; and
 - $\sigma_c \leq 0.04$ is required to ensure accurate distance measurement.

The redshift limit is defined as the maximum redshift of SNe passing these selection criteria.

The redshift of a complete sample, z_{complete} , is estimated from the redshift limit distribution, $z_{\text{lim,faint}}^{\text{SN}}$, of a simulated set of intrinsically faint SNe (i.e., those with $(x_1, c) = (-2.0, 0.2)$) with T_0 values spanning the season duration of a group of observations. The redshift completeness z_{complete} is defined as the 95th percentile of the $z_{\text{lim,faint}}^{\text{SN}}$ cumulative distribution.

The metrics are measured in HEALPix (Gorski et al. 2005) pixels of size 0.21 deg^2 ($n_{\text{side}} = 128$) over the region of the DDFs. For each pixel in the sky light curves are generated from observations of the simulated survey. Flux errors are estimated from the 5σ point-source limiting magnitude (5σ depth). The light curves are fitted (using the SALT2 model implemented in SNCosmo) to estimate the SN Ia parameters.

5. Analysis of LSST Simulations

The LSST project has periodically released sets of simulations containing a large number of survey strategies. The simulations analyzed in this section were performed with the Feature-based Scheduler (Naghib et al. 2019) based on a modified Markov decision process that maximizes the scientific outcome of the VRO during its 10-year survey. It allows a flexible approach for scheduling. The sequential decisions of which filter and which pointing to select are estimated from features (weather conditions/image depth, slew time, and footprint) to optimize the observing strategy. The output of the simulations is composed of a set of observing parameters¹⁸ estimated at the center of the field of view (FOV) of the telescope. These parameters serve as input for the generation of SN Ia light curves (Section 4).

The diversity of DD surveys proposed in LSST simulations is rather limited and we choose to analyze a representative set of DD surveys on the basis of the following criteria: number of visits (and filter allocation) per observing night, cadence of observation, dithering, and time budget. A list of the LSST simulated observing strategies considered in this study is given in Table 3.

Four sets of observing strategies can be defined from Table 3 according to the filter allocation per night, the parameter that has the most significant impact on the z_{complete} value: the *baseline-like* (11 observing strategies),

¹⁷ The phase is the number of rest-frame days relative to the *B*-band maximum luminosity.

¹⁸ The list of parameters is available at https://github.com/lsst/sims_featureScheduler.

Table 3
Survey Parameters for the Observing Strategies Analyzed in This Paper

Observing Strategy	Cadence (days)	N_{visits} $u/g/r/i/z/y$	Season Length (days)	Area (deg 2)	DD Budget (%)	Family
agnddf_v1.5_10yrs	2.0/2.0/2.0/2.0/2.0/2.0	0/1/1/3/5/4 [0.99–1]	164/165/235/189/171/177	112.9	3.4	agn
baseline_v1.5_10yrs	4.5/4.5/10.0/4.0/4.5/5.0	0/10/20/20/26/20 [0.28–0.43] 8/10/20/20/0/20 [0.56–0.71]	131/131/200/164/150/152	109.7	4.6	baseline
daily_ddf_v1.5_10yrs	2.0/2.0/2.0/2.0/2.0/2.0	0/1/1/2/2/2 [0.60–0.61] 1/1/1/2/0/2 [0.38–0.39]	161/161/236/188/171/178	113.5	5.5	daily
ddf_heavy_v1.6_10yrs	2.0/2.0/2.0/2.0/2.0/2.0	0/10/20/20/26/20 [0.26–0.39] 8/10/20/20/0/20 [0.60–0.72]	116/116/201/167/152/150	110.6	13.4	baseline
descddf_v1.5_10yrs	2.0/2.0/3.0/2.0/2.0/2.5	0/2/4/8/0/0 [0.37–0.5] 0/0/0/0/25/4 [0.30–0.38] 0/0/0/0/0/4 [0.19–0.25]	147/146/228/178/165/171	112.5	4.6	desc
dm_heavy_v1.6_10yrs	7.5/6.0/14.0/8.5/8.0/7.0	0/10/20/20/26/20 [0.31–0.45] 8/10/20/20/0/20 [0.54–0.68]	119/119/195/142/139/138	188.6	4.6	baseline
ddf_dither0.00_v1.7_10yrs	4.0/4.0/6.0/2.0/3.0/3.0	0/10/20/20/26/20 [0.17–0.43] 16/10/20/20/0/20 [0.56–0.81]	121/123/204/165/153/159 121/123/204/165/153/159	69.2 69.2	4.6 4.6	baseline
ddf_dither0.05_v1.7_10yrs	4.0/4.0/6.0/2.0/3.0/3.0	0/10/20/20/26/20 [0.16–0.42] 16/10/20/20/0/20 [0.57–0.83]	116/116/218/168/153/161	71.8	4.6	baseline
ddf_dither0.10_v1.7_10yrs	4.0/4.0/6.0/2.0/3.0/3.0	0/10/20/20/26/20 [0.19–0.43] 16/10/20/20/0/20 [0.57–0.81]	120/120/220/165/150/165	74.7	4.6	baseline
ddf_dither0.30_v1.7_10yrs	4.0/4.0/6.5/3.0/3.0/3.0	0/10/20/20/26/20 [0.21–0.45] 16/10/20/20/0/20 [0.54–0.78]	118/118/201/167/146/146	83.5	4.6	baseline
ddf_dither0.70_v1.7_10yrs	4.5/4.5/9.0/4.0/4.0/4.25	0/10/20/20/26/20 [0.19–0.43] 16/10/20/20/0/20 [0.57–0.79]	123/137/201/163/146/146	104.5	4.6	baseline
ddf_dither1.00_v1.7_10yrs	4.0/4.0/14.0/5.5/5.0/5.0	0/10/20/20/26/20 [0.23–0.43] 16/10/20/20/0/20 [0.56–0.77]	113/118/198/153/143/143	124.4	4.6	baseline
ddf_dither1.50_v1.7_10yrs	4.5/4.5/16.5/8.5/6.75/6.0	0/10/20/20/26/20 [0.20–0.42] 16/10/20/20/0/20 [0.57–0.79]	121/121/196/145/135/139	159.3	4.6	baseline
ddf_dither2.00_v1.7_10yrs	4.0/4.0/19.0/12.0/9.5/9.0	0/10/20/20/26/20 [27–44] 16/10/20/20/0/20 [0.57–0.79]	112/111/193/137/118/133	199.3	4.6	baseline

Notes. For the cadence and season length, the numbers correspond to the ADFS1/ADFS2/CDF-S/COSMOS/ELAIS/XMM-LSS fields, respectively. The numbers following the filter allocation (N_{visits} column) are the minimum and maximum mean fraction of visits (per field over seasons) in the filter distribution. Only filter combinations with a contribution higher than 0.01 are considered.

agn, *daily*, and *desc* families. We estimate the pair metric ($N_{\text{SN}}^{z \leq z_{\text{complete}}}$, z_{complete}) (defined in Section 4) for these families. $N_{\text{SN}}^{z \leq z_{\text{complete}}}$ is estimated for median SNe Ia with $(x_1, c) = (0.0, 0.0)$ to speed up processing. Figure 5 shows that higher redshift limits are reached for the *baseline-like* family. Most (10/11) of these observing strategies reach $z_{\text{complete}} \sim 0.65$. The *ddf_heavy* strategy, the one with the largest DD time budget, reaches $z_{\text{complete}} \sim 0.72$ and also collects the largest number of well-measured SNe Ia. The *daily* and *desc* families are characterized by a shallower depth but by a significant number of well-measured SNe Ia.

The metric output ($N_{\text{SN}}^{z \leq z_{\text{complete}}}$, z_{complete}) (see Appendix A for more details) is driven by the probability of an SN Ia light curve fulfilling the requirements defined in Section 4. This observing efficiency depends on S/N^b, which is defined by the sampling frequency of the light-curve points. The number of well-measured SNe Ia is thus strongly dependent on the cadence of observation, as illustrated in Figure 6

(top): as expected, higher cadences lead to higher ($N_{\text{SN}}^{z \leq z_{\text{complete}}}$, z_{complete}).

The observing strategies studied in this paper are characterized by a wide range of cadences (Figure 6, top). Only two surveys, *ddf_heavy* and *daily*, have more than 50% of their observations having a 1 day cadence (Table 4). The *baseline* and *dither0.00* surveys, the two strategies with the lowest $N_{\text{SN}}^{z \leq z_{\text{complete}}}$, present a large fraction of observations with a cadence of at least 3 days. These cadence distributions can be explained by some period with no observations. Two sources of gaps can be identified. One is the telescope downtime due to clouds and/or telescope maintenance. The other is the scanning strategy, where choices have to be made on which fields are to be observed on a given night. Internight gaps arising from telescope downtime lead to about 16%–20% of nights without observation per season and are not expected to exceed a few days (except for longer maintenance periods, which could last up to 16 days; see Section 9). But the cadence may significantly

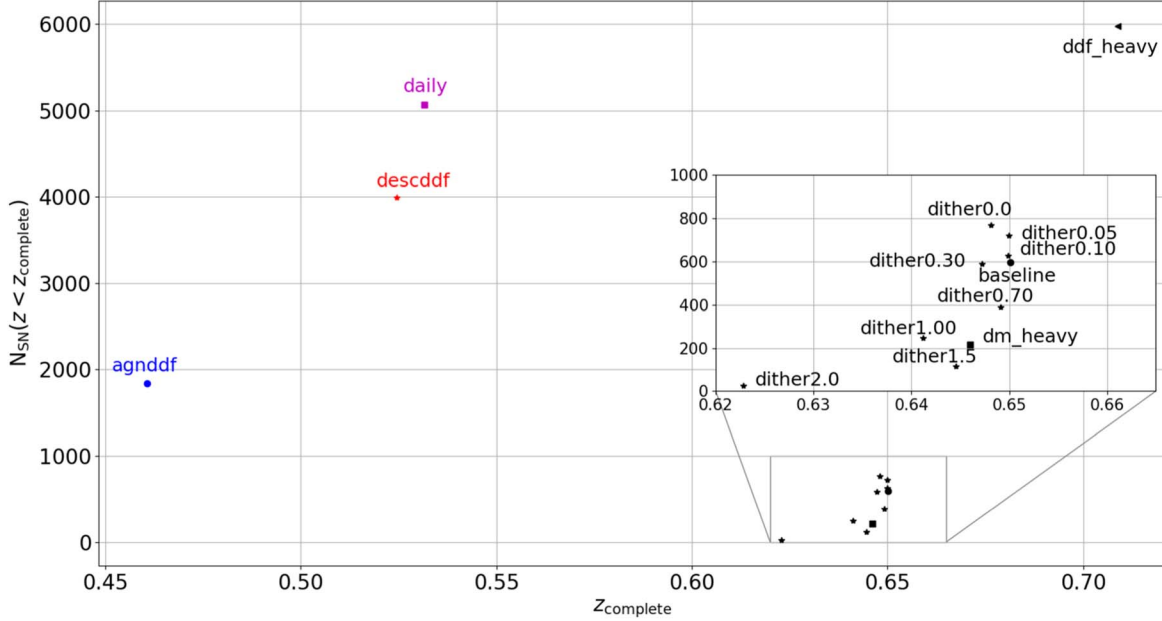


Figure 5. $N_{\text{SN}}(z \leq z_{\text{complete}})$ vs. z_{complete} for the LSST simulated observing strategies considered in this paper.

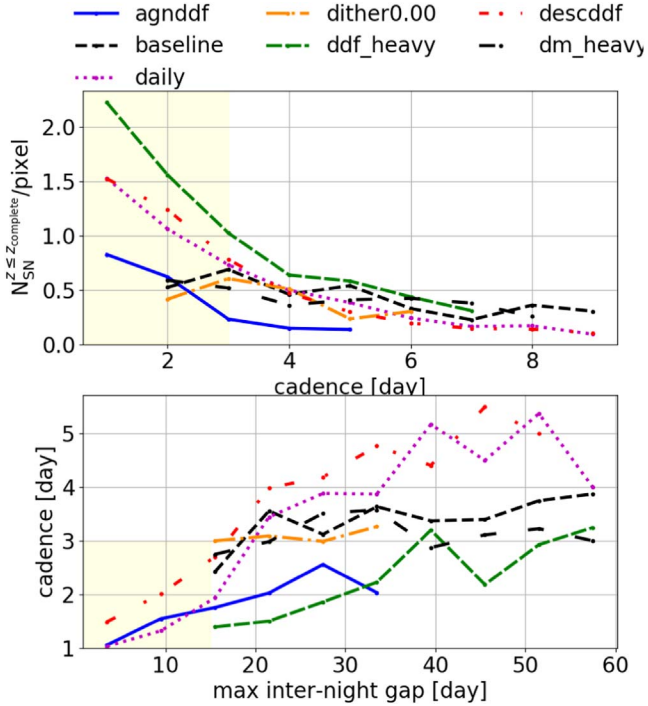


Figure 6. Median number of well-measured SNe $N_{\text{SN}}^{z \leq z_{\text{complete}}}$ (per pixel of 0.21 deg^2) as a function of the cadence of observation (top) and median cadence as a function of maximal inter-night gap (bottom) for a set of LSST simulated strategies studied in this paper. Yellow areas correspond to observing strategy parameters (cadence and maximal inter-night gaps) leading to a high-quality SN Ia sample.

increase for gaps longer than ~ 10 days. Large gaps of a few tens of days lead to a dramatic decrease in the cadence of observation, as illustrated in Figure 6 (bottom).

The VRO will provide a combination of large-scale dithers at each point of observation. Dithering patterns are composed of translational and rotational dithers (Awan et al. 2016). The former correspond to offsets of the telescope pointings, the latter to offsets of the camera rotational angles. We study the

Table 4
Cadence Distribution for a Set of Strategies Studied in This Paper

Strategy	Cadence				
	1 day	2 days	3 days	4 days	≥ 5 days
agnddf	37.6%	56.5%	5.0%	0.7%	0.1%
baseline	0.0%	28.8%	44.7%	11.9%	14.6%
daily	56.4%	21.2%	11.2%	5.6%	5.6%
dither0.00	0.0%	36.1%	43.7%	14.4%	5.8%
ddf_heavy	62.4%	22.8%	10.5%	3.2%	1.1%
descddf	9.9%	58.9%	16.4%	7.0%	7.8%
dm_heavy	0.0%	31.0%	39.3%	18.4%	11.2%

Note. The cadence is estimated from the nightly visits corresponding to all the filters *grizy* for all the strategies but descddf, which is characterized by observations related to *gri* and *zy* filters nightly interleaved (i.e., *gri* visits one night and *zy* visits the night after).

impact of the translational dithering on the metrics. It is expected to affect both the number of well-measured SNe and the redshift completeness for each of the pixels of the field. With no dithering, the $N_{\text{SN}}^{z \leq z_{\text{complete}}}$ and z_{complete} distributions are uniform across the whole field area. The translational dithering has an impact on edge pixels, which are thus characterized by a lower cadence with respect to central pixels. A decrease in both $N_{\text{SN}}^{z \leq z_{\text{complete}}}$ and z_{complete} (per pixel) is then observed for edge pixels. The redshift completeness z_{complete} tends to decrease with an increase of the translational dither offset (tdo), with a greater effect for high cadences. The number of SNe is a result of the trade-off between two effects (Figure 7): an increase of the survey area (which increases with tdo) and a decrease of the cadence (which decreases with tdo). An increase of the survey area leads to an increase of the number of SNe for high cadences and low tdo values.

In summary, the LSST simulated strategies lead to the observation of a sample of well-measured SNe Ia with a rather low z_{complete} , the redshift limit of the complete cosmology-grade SN Ia sample. It will be shown in the following

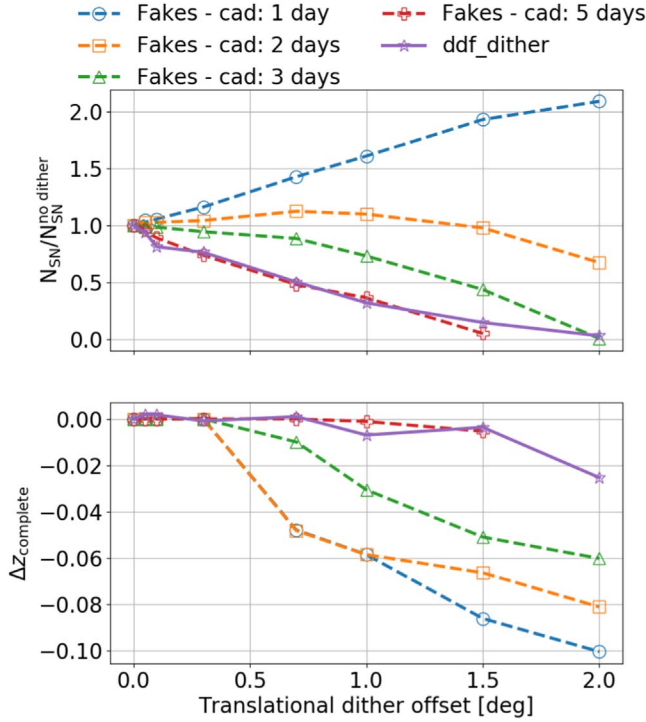


Figure 7. Ratio of the number of SNe $N_{\text{SN}}/N_{\text{SN}}^{\text{no dither}}$ (top) and z_{complete} difference (bottom) as a function of tdo. The simulations labeled “Fakes” (dashed lines) correspond to regular cadences (1, 2, 3, and 5 days) with median observing conditions (5σ depths in single exposures of 24.13/23.84/23.45/22.74/22.10 for the $g/r/i/y/z$ bands, respectively, and a season length equal to 180 days). We choose a random dithering from one visit to another. The results presented in this figure may depend on the dithering pattern.

(Section 7) that reaching $z_{\text{complete}} \sim 0.6$ is not sufficient to achieve a measurement of w with a high degree of precision. The redshift completeness z_{complete} is mainly driven by the S/N^b values (Equation (3)), which depend on the number of visits in the corresponding band N_{visits}^b (Section 6). The number of visits per band thus has to be increased to reach higher z_{complete} . We propose in Section 6 a method for assessing the relationship between N_{visits}^b and z_{complete} . The second conclusion of these studies is that the cadence is a key parameter to collecting a large sample of well-measured SNe Ia. High cadences are favored to maximize S/N^b . Large internight gaps are undesirable as they lead to a decrease of the number of well-measured SNe. It is critical to reduce internight gaps originating from the survey strategy so as to maximize the size and depth of the well-measured SN Ia sample. Finally, larger translational dithers reduce the DDF area with high cadence and lead to a dramatic decrease of the number of well-measured SNe Ia for low-cadence ($\gtrsim 3$ days) strategies.

6. Optimization of the Number of Visits

The analysis of LSST simulations has shown (see Section 5) that it seems difficult to collect complete samples of SNe Ia with redshift higher than $z_{\text{complete}} \sim 0.55\text{--}0.65$. The proposed cadences of observation, filter allocations, and season lengths do not produce higher-redshift DD surveys if the DD time budget is limited to $\sim 5\%$. According to Equation (4), reaching higher z_{complete} requires increasing S/N^b .

S/N^b is the complex result of the combination of the SN Ia flux distribution per filter (z -dependent), the number of visits per band, the cadence of observation, and the observing

conditions (5σ depth). It is thus not possible to estimate the observing strategy parameters required to reach higher redshifts from the results of Section 5 (by a simple rescaling for instance). This is why we present in this section a study to assess the relationship between the redshift completeness and the number of visits per band and per observing night (for a defined cadence). The optimized number of visits per band required to reach higher redshifts estimated with this approach is a key parameter to building DD surveys consistent with the list of constraints presented in Section 2 and in Section 3.

As described in Equation (5) the DD time budget depends primarily on five parameters: the number of fields to observe, the season length (per field and per season), the number of seasons of observation (per field), the cadence of observation (per field and per season), and the number of visits N_{visits}^b per filter and per observing night. N_{visits}^b is related to S/N^b through the flux measurement uncertainties σ_i^b . In the background-dominated regime one has $\sigma_i^b \simeq \sigma_5^b$, where σ_5^b is equal by definition to

$$\sigma_5^b = \frac{f_5^b}{5} \quad (7)$$

where f_5^b is the 5σ flux related to the 5σ depth magnitude m_5^b through

$$m_5^b = -2.5 \log f_5^b + zp^b \quad (8)$$

where zp^b is the zero-point of the considered filter. The magnitude m_5^b is related to N_{visits}^b through

$$m_5^b - m_5^{b,\text{single}} \approx 1.25 \log(N_{\text{visits}}^b) \quad (9)$$

where $m_5^{b,\text{single}}$ is the 5σ depth corresponding to a single visit, a parameter depending on the observing conditions. Equations (7)–(9) describe the relationship between S/N^b and N_{visits}^b . The requirement $S/N^b \geq S/N_{\text{min}}^b$ is equivalent to $N_{\text{visits}}^b \geq N_{\text{visits,min}}^b$ and Equation (4) may be written as

$$\wedge(N_{\text{visits}}^b \geq N_{\text{visits,min}}^b) \Rightarrow \sigma_c \leq 0.04 \Rightarrow z_{\text{lim}}. \quad (10)$$

Equations (4) and (10) are satisfied by many different S/N^b (N_{visits}^b) combinations and constraints have to be applied to choose optimal configurations.

We use the following method to estimate $N_{\text{visits}}^b(z)$. A systematic scan of the S/N parameter space (S/N^g , S/N^r , S/N^i , S/N^z , and S/N^y) is performed. Median observing conditions estimated from the DD simulations are used, namely $m_5^{g,\text{single}} = 24.48$, $m_5^{r,\text{single}} = 23.60$, $m_5^{i,\text{single}} = 24.03$, $m_5^{z,\text{single}} = 22.97$, and $m_5^{y,\text{single}} = 22.14$. For each S/N combination and for a set of cadences (1 day to 4 days), light curves of an intrinsically faint SN Ia (i.e., one with $x_1 = -2.0$, $c = 0.2$) in the redshift range [0.01, 1.0] are simulated using light-curve templates (that we have generated with SNCosmo) and the SN Ia parameter errors (σ_c , σ_{x_1}) are estimated using the Fisher matrix formalism. This approach considerably reduces the processing time (as compared to the full simulation+fit) while ensuring the highest degree of accuracy of the light-curve points (fluxes and flux errors) and of the SN parameter errors. The light curves fulfilling the requirements defined in Section 4 are used to define the S/N parameter space, or equivalently the N_{visits} parameter space (N_{visits}^g , N_{visits}^r , N_{visits}^i , N_{visits}^z , and N_{visits}^y) according to Equation (10), corresponding to well-measured SNe Ia. Optimal combinations are selected

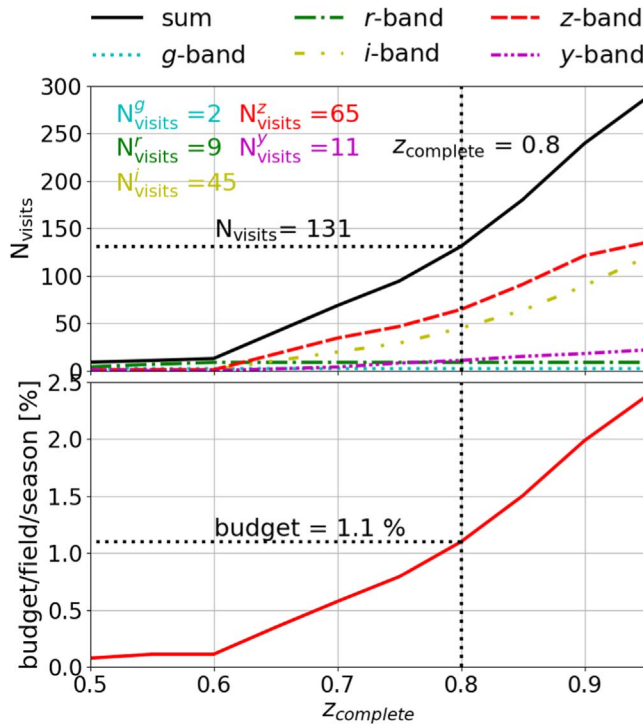


Figure 8. Top: Number of visits per observing night as a function of the redshift completeness. A total of 131 visits with the filter allocation ($N_g^{\text{visits}}, N_r^{\text{visits}}, N_i^{\text{visits}}, N_z^{\text{visits}}, N_y^{\text{visits}}$) = (2, 9, 45, 64, 11) are required per observing night to reach $z_{\text{complete}} \sim 0.8$ for a cadence of 1 day. Bottom: Time budget per field and per season of observation as a function of z_{complete} . A 1 day cadence and a season length of 180 days are assumed. Observing a field every night for 180 days with a redshift completeness of 0.80 corresponds to a time budget of 1.1%. For a DD survey with five fields observed for 10 yr (the current proposed strategy; see Section 5), this would correspond to a DD time budget of 40%.

by minimizing the total number of visits per observing night and by requiring a maximum number of y-band visits. This selection aims at reducing (potentially severe) systematic effects on the y-band measurements (High et al. 2010). Dedicated studies (beyond the scope of this paper) would be needed to assess the impact of photometric calibration using wavelength-dependent methods such as the “ubercal-like” methods used with success to calibrate wide-field surveys (Padmanabhan et al. 2008; Regnault et al. 2009; Schlaflay et al. 2012; Magnier et al. 2020) or forward calibration methods such as the forward global photometric calibration (Burke et al. 2017) used within the Dark Energy Survey.

The result is displayed in Figure 8 (top) for a 1 day cadence. The number of visits strongly increases with the redshift completeness for $z_{\text{complete}} \gtrsim 0.7$, where only three bands (izy) can be used to construct SN Ia light curves. About 130 visits (1 hr and 5 minutes of observation) are required to reach $z_{\text{complete}} \sim 0.8$ for a 1 day cadence. Since the number of visits required to reach a given z_{complete} value increases linearly (as a first approximation) with the cadence, this corresponds to ~ 3.25 hr of exposure time per night for a 3 day cadence.

It is known that the rest-frame UV region is subject to large fluctuations between SNe Ia in the SALT2 light-curve model (see Section 4). One of the consequences is that only three bands (izy) and two bands (zy) may be used to reconstruct light curves for redshifts higher than ~ 0.7 and ~ 1.1 , respectively. The SN Ia parameter errors depend on the S/N values, but also on the shape of the light curves per band. The contribution of S/N^y to the SN Ia parameter errors tends to increase with

Table 5
A Set of Optimal Numbers of y-band Visits as a Function of z_{complete}

z_{complete}	0.65	0.70	0.75	0.80	0.85	0.90
N_y^{visits}	3	7	16	21	30	38

z_{complete} if the total number of visits remains relatively constant. A high N_y^{visits} for low z_{complete} (~ 0.7) leads to a net loss of well-measured SNe Ia because of bad color measurements. The optimal N_y^{visits} as a function of z_{complete} is estimated by computing the redshift limit of the median SN Ia (i.e., with $(x_1, c) = (0.0, 0.0)$) in configurations with $5 \leq N_y^{\text{visits}} \leq 80$. Requiring a z_{lim} variation lower than 0.01 leads to the results of Table 5.

It is possible to estimate the budget per field and per season of observation as a function of z_{complete} by using Equation (5) and the results of Figure 8 (top). As expected (Figure 8, bottom) a significant increase is observed for higher redshifts and the observation of a field for 180 days with $z_{\text{complete}} \sim 0.9$ requires a time budget of 2.

We quantify the impact of the SALT3 model by estimating z_{complete} using the number of visits (Figure 8) estimated with the SALT2 model and similar observing conditions. A slight improvement is observed (Figure B1 in Appendix B): $\Delta z_{\text{complete}} \sim 0.03$ for $z_{\text{complete}} \sim 0.9$. It may be explained by the new features of the SALT3 model (extended wavelength range and reduced uncertainties as compared to SALT2) (Kenworthy et al. 2021).

The optimized number of visits required to reach higher redshift completeness is the last piece of the puzzle to be included in the time budget estimator (Equation (5)). We have now the tools to design realistic and optimal DD surveys.

7. Optimal LSST DD Surveys for Cosmology with SNe Ia

In the following, we examine three key points of the surveys (redshift completeness, cadence of observation, and cosmological measurements) before presenting a set of optimized scenarios.

Redshift completeness and host spectroscopic z. Spectroscopic data sets from cosmological endeavors overlapping with LSST in area and timing are essential for SN Ia cosmology. They provide enormous added benefits through (a) the follow-up of a subset of the full sample of well-measured SNe (to improve the models used to build training samples for photometric classification), and (b) the measurement of host galaxy redshifts with high accuracy. An optimal DD survey requires maximizing the fraction of observed SNe Ia with host galaxy spectroscopic z measurement to minimize the impact of photo- z errors. This is all the more important for higher- z SNe Ia, which significantly contribute to the measurement of cosmological parameters. It is thus critical to take into account available host spectroscopic measurements when designing optimized DD scenarios with higher z_{complete} .

Three spectroscopic resources contemporaneous with LSST—the Dark Energy Spectroscopic Instrument (DESI; DESI Collaboration et al. 2016), the Primary Focus Spectrograph (PFS/Subaru; Tamura et al. 2016), and 4MOST (de Jong et al. 2019)—will provide vital live spectra and host spectroscopic redshifts (Mandelbaum et al. 2019).

DESI is a ground-based dark energy experiment used to conduct a five-year survey that will cover $14,000 \text{ deg}^2$. More than 30 million (20 million with $z > 0.5$) galaxy and quasar

redshifts will be measured to study baryon acoustic oscillation and the growth of structures through redshift-space distortions. The DESI survey will overlap with at least 4000 deg² of the LSST footprint in the northern hemisphere.

The PFS/Subaru spectroscopic follow-up survey is designed to observe two LSST DDFs accessible from the Subaru telescope: COSMOS and XMM-LSS. About 2000 spectra of live SNe and 20,000 host galaxy redshifts up to $z \sim 0.8$ will be collected after 10 years.

The 4MOST Time-domain Extragalactic Survey (TiDES; Swann et al. 2019) is dedicated to the spectroscopic follow-up of extragalactic optical transients and variable sources selected from, e.g., LSST. The goal is to collect spectra for up to 30,000 live transients to $z \sim 0.5$ and to measure up to 50,000 host galaxy redshifts up to $z \sim 1$. This corresponds to both the DD and the WFD fields.

Two sets of LSST fields may then be defined to fully benefit from the synergy with DESI, PFS/Subaru, and 4MOST. DESI and PFS/Subaru will provide live spectra and spectroscopic redshifts for the northernmost fields, COSMOS and XMM-LSS, over a broad range of redshifts. Southern fields—Euclid/Roman, CDF-S, and ELAIS-S1—will benefit from 4MOST/TIDES measurements.

Cadence of observation. Several important arguments can be put forward in favor of high cadences: the total number of visits per night, the season length, the translational dithering, and internight gaps.

More than 240 visits are required to reach $z_{\text{complete}} \geq 0.9$ for a 1 day cadence (Figure 8, top). The same depth is obtained for a 3 day cadence with more than 720 visits, which is about 6 hr of observation. Reaching higher z_{complete} with low-cadence observing strategies is thus not realistic: it would potentially jeopardize the uniformity of the WFD survey.

Because of their northernmost positions, COSMOS and XMM-LSS are characterized by shorter season lengths with respect to other fields (for the same observing time per night) (Figure 3). Requiring more than 480 visits per night (to reach $z_{\text{complete}} \geq 0.9$ with a 2 day cadence) would dramatically degrade the season lengths (to less than 90 days for these two fields) and would drastically reduce the size of the well-measured SN sample (by more than 50%).

As shown in Figure 7 the translational dithering has a limited impact on the number of well-measured SNe Ia and on z_{complete} up to $\text{tdo} \sim 1$ degree for high cadences. The number of well-measured SNe Ia falls rapidly with tdo for cadences lower than 3 days.

One of the main conclusions of the analysis of the proposed LSST simulations (Section 5) is that large internight gaps have undesirable effects on the sampling and on the quality of SN Ia light curves. They can be reduced to a minimum (i.e., to unavoidable gaps related to telescope maintenance or bad weather conditions) by either observing DDFs at high cadences or including a mechanism in the scheduler that would maintain a high observing rate of SNe Ia (see Section 9 for suggestions).

Cosmological metric. The most accurate way to measure cosmological parameters from a sample of well-measured SNe Ia is to perform a maximum likelihood analysis by minimization:

$$-\ln \mathcal{L} = (\mu - \mu_{\text{th}}(z, \Omega_m, w))^{\top} C(\mu - \mu_{\text{th}}(z, \Omega_m, w)) \quad (11)$$

where C is the covariance matrix and μ is the distance modulus (Equation (1)). The variable $\mu_{\text{th}}(z, \Omega_m, w)$ is defined by

$$\mu_{\text{th}}(z, \Omega_m, w) = 5 \log_{10}[d_L(\text{Mpc})] + 25. \quad (12)$$

In a flat universe, the luminosity distance d_L is defined by

$$d_L(z, \Omega_m, w) = \frac{c(z+1)}{H_0} \int_0^z \frac{dz'}{\sqrt{(1 - \Omega_m) + \Omega_m(1+z')^{3w}}} \quad (13)$$

where Ω_m is the dark matter density parameter, and w is the parameter of the dark energy equation of state. Five parameters are to be estimated: the cosmological parameters (Ω_m and w) and the nuisance parameters (M , α , and β) (Equation (1)).

The goal of this section is to study a large set of surveys by varying the number of fields to be observed, the redshift completeness (i.e., by having samples with redshift completeness that is field-dependent), and the number of seasons. Using the abovementioned method for each scenario would require producing a lot of (time-consuming) simulations and fits of SN Ia light curves to estimate cosmological parameters. We thus choose to work with the distance moduli of the SNe simulated using

$$\mu_i(z_i) \sim \mathcal{N}(\mu_{\text{th}}(z_i, \Omega_m, w), \sigma^2 = \sigma_{\mu_i}^2 + \sigma_{\text{int}}^2 + \sigma_{\text{syst}_i}^2) \quad (14)$$

where σ_{int} is the intrinsic dispersion of SNe ($\sigma_{\text{int}} \sim 0.12$) and σ_{syst} accounts for systematic uncertainties related to Malmquist bias ($\sigma_{\mu}^{\text{bias}} \lesssim 0.06$), photometric calibration (a few millimagitudes) (these estimations are from Brout et al. 2019), photo-z measurements ($\sigma_{\mu}^{\text{phot-z}} \lesssim 0.10$), or SN modeling. The error $\sigma_{\mu}(z)$ is the distance modulus error for each SN Ia of redshift z_i . It is estimated from a complete simulation of DD surveys with varying z_{complete} using the method developed in Section 4.

The cosmological parameters are estimated by minimization:

$$-\ln \mathcal{L} = \sum_{i=1}^{N_{\text{SN}}} \frac{(\mu_i - \mu_{\text{th}}(z_i, \Omega_m, w))^2}{\sigma_{\mu_i}^2 + \sigma_{\text{int}}^2 + \sigma_{\text{syst}_i}^2} \quad (15)$$

where N_{SN} is the number of well-measured SNe Ia used to perform the fit. The realistic simulations used to estimate σ_{μ} and N_{SN} take into account redshift bias (see Appendix C for more details). Concerning the (x_1, c) distribution of SNe Ia, we use the G10 intrinsic scatter model (Scolnic & Kessler 2016), where (x_1, c) distributions are asymmetric Gaussian distributions with three parameters. For each DD survey considered in the following, a sample of about 100,000 low- z SNe Ia (10,000 per year) is added up to $z_{\text{complete}} \sim 0.2$ for the WFD survey (Lochner et al. 2022).

The following sections describe a set of optimized scenarios based on two different approaches. One is optimizing the number of well-measured SNe Ia collected by the survey. The other aims at probing high redshift completeness domains. A survey is characterized by three parameters: the redshift completeness, the number of DDFs, and the cadence of observation. Three metrics are presented to assess the proposed scenario: the DD time budget, the cosmological metric (we choose the error on the w parameter, σ_w), and the total number of well-measured SNe Ia. Only statistical errors are included for the results presented in Section 7.1 and Section 7.2.

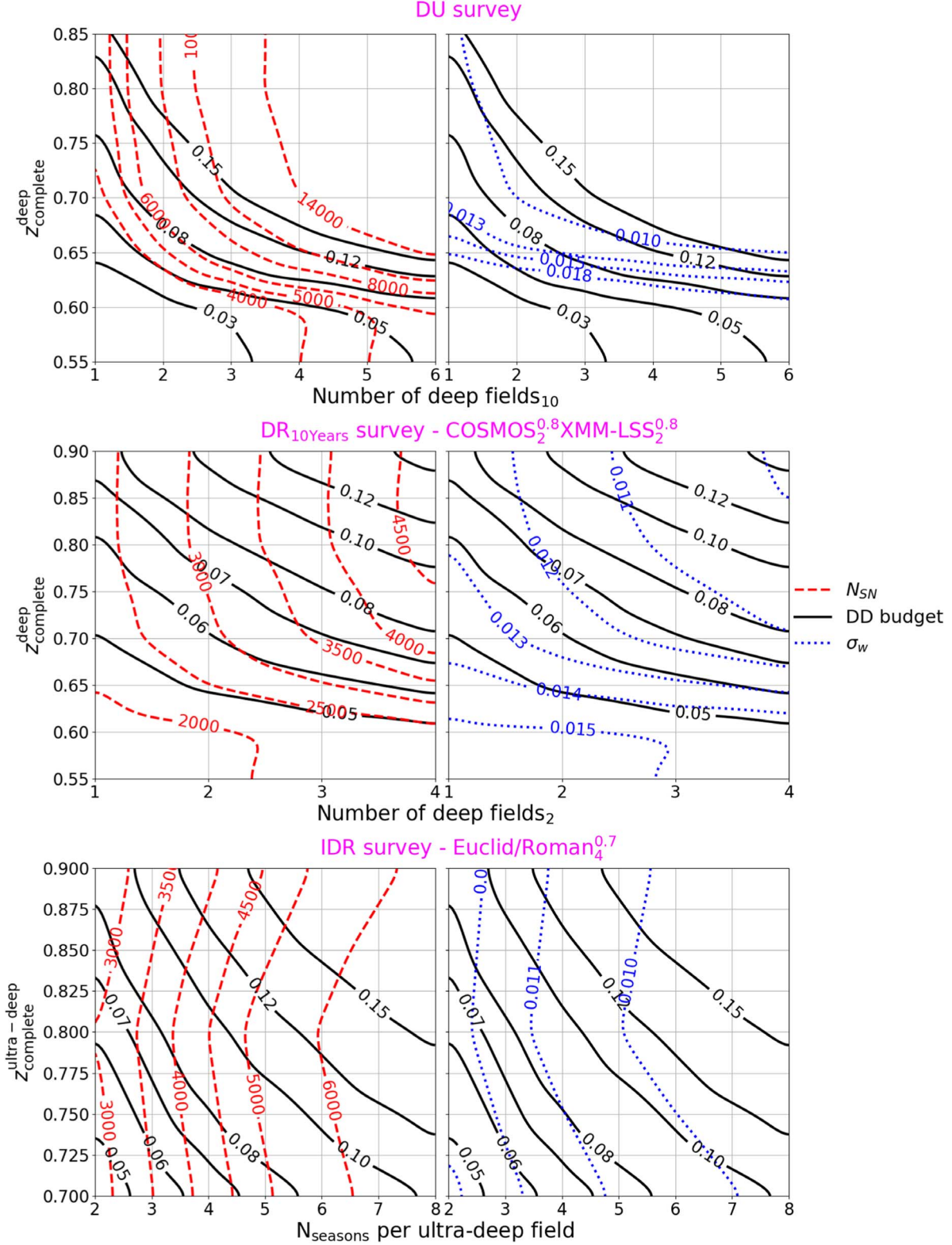


Figure 9. N_{SN} (red dashed lines), DD time budget (black solid lines), and σ_w (blue dotted lines) for three types of surveys: DU (top), deep rolling (DR) 10 yr (middle), and intensive DR (IDR) (bottom). Subscripts correspond to the number of seasons of observation (6 month season length) and superscripts to the redshift completeness. The number of y -band visits is less than 20 (per observing night). Only statistical uncertainties are included.

7.1. Deep Universal Surveys

In the deep universal (DU) survey, all the DDFs are observed for 10 yr with a similar cadence, season length, and z_{complete} (i.e., a similar number of visits per band and per observing

night). The time budget is the major factor limiting the redshift completeness of the survey (Figure 9, top). A time budget higher than 15% is required to reach $z_{\text{complete}} \lesssim 0.65$ with five DDFs (with two VRO pointings for Euclid/Roman). This configuration leads to a high number of well-measured SNe Ia ($\sim 14,000$)

and to the best cosmological constraints ($\sigma_w \sim 1\%$) from the DU strategies we consider. The parameters z_{complete} and N_{SN} dramatically decrease for a time budget lower than 5% and the cosmological measurements get significantly worse ($\sigma_w \geq 2\%$).

Cadence of observation. A $z_{\text{complete}} \sim 0.65$ can be achieved with 41 visits per night of observation with a 1 day cadence (Section 6). Up to four fields (because of its northernmost location, COSMOS is visible independently of the other DDFs) may have to be scanned for some nights, which corresponds to 1 hr and 42 minutes of observation. Changing to a 3 day cadence would require 123 visits per field and per night of observation. In that case the scanning of four fields (five pointings) has to be spread over three nights with at least two fields observed per night. This corresponds to about 2 hr of observation.

7.2. DR Surveys

Observing five fields for 10 yr up to $z_{\text{complete}} \sim 0.9$ would certainly give access to a large sample of well-measured SNe Ia (around 19,000) but also to an unrealistic scenario ($N_{\text{visits}}^{\text{DD}} \gtrsim N_{\text{visits}}^{\text{WFD}}$). The only way to reach higher z_{complete} while remaining within a reasonable budgetary envelope is to reduce the number of fields to be observed and/or the number of seasons of observation. We propose the DR strategy characterized by a limited number of seasons of observation per field (at least two) and a large number of visits per observing night (more than 130 for higher z_{complete}).

A realistic large-scale high- z DR survey is characterized by (a) a high cadence of observation (1 day), (b) a rolling strategy (with a minimum of two seasons of observation per field), and (c) two sets of fields, ultradeep (COSMOS and XMM-LSS, with $z_{\text{complete}} \gtrsim 0.8$) and deep (Euclid/Roman, CDF-S, and ELAIS-S1, with $z_{\text{complete}} \gtrsim 0.7$) fields. We study two DR surveys in the following, characterized by a minimal number of seasons of observation per field or by a minimal number of fields to be observed.

7.2.1. DR 10 yr

In this scenario all the DDFs are observed for two seasons. The results of the triplet (time budget, σ_w , N_{SN}) as a function of the number of DDFs and redshift completeness are given in Figure 9 (middle). It seems difficult, with a time budget lower than 5%, to perform cosmological measurements of w with an accuracy better than 1.5%. A sample of ~ 4000 –4500 well-measured SNe Ia with a reasonable time budget of $\sim 8\%$ would lead to $\sigma_w \sim 1.1\%$.

This scenario appears to have two essential weaknesses. The number of seasons of observation per field is low. Periods of bad weather could affect the progress of the survey and the quality of the SN Ia sample. What is more, this survey requires a precise timeline that may be difficult to tune (see an example below).

The sequence of observations (field/night) of the DR survey must fulfill a couple of constraints. LSST observation of Euclid/Roman has to be contemporaneous with Euclid (years 2 and 3) and with the Roman Space Telescope (years 5 and 6). Observing multiple fields per night is not optimal if the number of visits per field is high. It may jeopardize the uniformity of the WFD survey (if the total number of DD visits is too high) and may have a negative impact on the regularity of the DD cadence (if a choice has to be made among the DDFs). Overlap

of field observations should thus be minimized. This means that the DR survey should be deterministic, that is, having a time observation scheduling defined in advance. An example of the progress of a DR survey is given in Figure 10 for a configuration of five fields, a cadence of 1 day, and a survey complete up to $z \lesssim 0.8$ and $z \lesssim 0.7$ for ultradeep (131 visits per observing night) and deep fields (68 visits per observing night), respectively.

7.2.2. IDR

In this scenario a minimal number of fields are observed and the goal is to maximize the redshift completeness of the survey, defined as the median redshift completeness of the observed fields. The choice of fields may be motivated by the following considerations: the need to explore high redshift completeness domains, and synergy with surveys contemporaneous with VRO operations. Fulfilling these requirements leads to a choice of three fields: COSMOS, XMM-LSS, and Euclid/Roman. In this scenario Euclid/Roman is observed for four seasons up to $z_{\text{complete}} \sim 0.7$ and COSMOS and XMM-LSS are observed every year with a redshift completeness of at least 0.7. Reaching higher- z_{complete} domains means increasing the number of visits per observing night (~ 130 visits to reach $z_{\text{complete}} \sim 0.8$ for a 1 day cadence). The DD time budget may then be used up in just a few years and this is why this scenario may be dubbed “intensive.” The results of the triplet (time budget, σ_w , N_{SN}) as a function of the number of seasons of observation and the redshift completeness of the two ultradeep fields are given in Figure 9 (bottom). About 3500–4000 well-measured SNe Ia are collected after 3–4 yr of observation of COSMOS and XMM-LSS up to $z_{\text{complete}} \lesssim 0.8$. The corresponding time budget is 8% and $\sigma_w \sim 1.1$ –1.2.

7.3. Conclusion: DR and IDR Surveys Yield More Accurate Cosmological Measurements

Some conclusions can be drawn from a comparison of the surveys presented in Section 7.1 and Section 7.2:

- Redshift completeness.* It is impossible to reach $z_{\text{complete}} \geq 0.6$ –0.65 for DU surveys. This can be explained by the DD time budget envelope leading to a limited number of visits per observing night if a large number of fields are observed for all seasons for 10 yr. This results in a low number of visits in the redder bands (z and y) imposing a limit on z_{complete} .
- Accuracy of cosmological measurements.* Under the assumption of an identical time budget, IDR surveys lead to more accurate cosmological measurements. With a DD time budget of 5%, the w parameter can be measured with $\sigma_w \sim 1.3\%$ –1.4% for IDR scenarios and to $\sigma_w \geq 2\%$ for DU surveys. This result is mainly due to the fact that the distribution of the number of SNe Ia $N(z)$ depends on the redshift completeness value of the survey (see Figure C1 in Appendix C). IDR surveys present a higher fraction of SNe Ia at higher redshift compared to DU surveys (Figure 11) and lead to more accurate cosmological measurements.
- DD time budget impact.* Moving from a time budget of 5% to 8% would lead to a relative decrease in σ_w of 20%–25%, depending on the scenario. Measuring w with a precision of $\sim 1.1\%$ requires a minimal time budget of 8% and 15% for DR and DU scenarios, respectively.

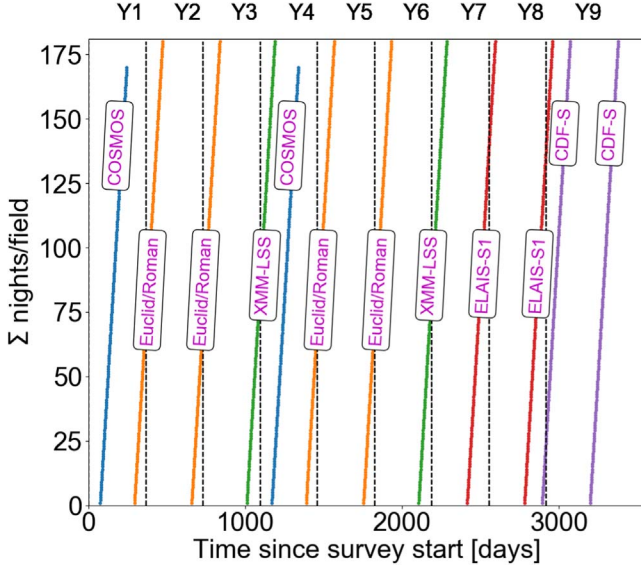


Figure 10. Cumulative sum of the number of nights (per field and per season) as a function of the time since the survey start (assumed to be late 2023). The following sequence of observations is considered: COSMOS, Euclid/Roman ($\times 2$), XMM-LSS, COSMOS, Euclid/Roman ($\times 2$), XMM-LSS, ELAIS-S1 ($\times 2$), and CDF-S ($\times 2$), with a maximum season length of 180 days for the deep fields, a cadence of 1 day, and only one field observed per night. The fields are required to be observable (airmass ≤ 1.5 and $20^\circ \leq \text{altitude} \leq 86.5^\circ$) for at least 1 hr and 5 minutes (131 visits) for the ultradeep fields and for at least 34 minutes (68 visits) for the deep fields. The overlap, defined as the fraction of nights with more than one field observed, is $\sim 4\%$.

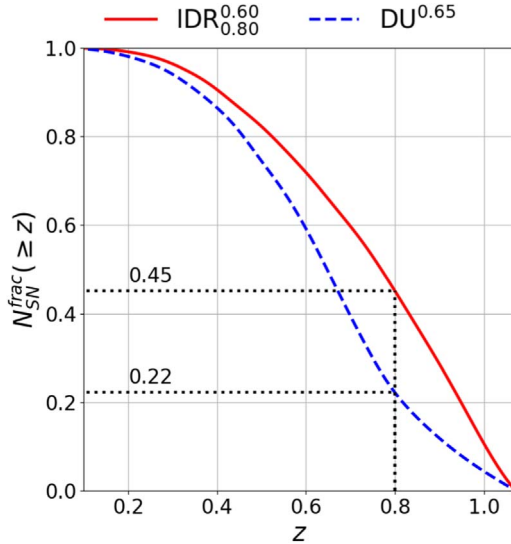


Figure 11. Fraction of SNe Ia ($\geq z$) as a function of the redshift (z) for two scenarios: IDR $_{0.60}^{0.80}$ (full red line) and DU $^{0.65}$ (dashed blue line). The fraction of SNe Ia with $z \geq 0.8$ is 45% and 22% for the IDR $_{0.60}^{0.80}$ and DU $^{0.65}$ surveys, respectively.

8. Realistic Surveys—Impact of Host Galaxy Redshifts

The goal of this section is to draw a comparison of the performance of realistic surveys using the triplet (time budget, σ_w , N_{SN}). The effects of two critical aspects have to be included to get a more accurate comparison of the proposed surveys: those of the Malmquist bias correction and those of the SNIa host galaxy redshift estimation.

Systematic uncertainties related to observational selection effects will probably account for a major part of the error

budget in the era of LSST. We consider two components related to the selection bias: a statistical contribution, related to the limited number of SNe Ia per redshift bin, and a bias contribution, due to the (limited) knowledge of the (x_1, c) distribution of the selected SNe Ia. We use the G10 intrinsic scatter model (Scolnic & Kessler 2016), where distributions are asymmetric Gaussian distributions with three parameters and their uncertainties σ . We perform simulations by individually varying each parameter by $\pm 1\sigma$. The differences of the distance modulus values with respect to the nominal configuration are added quadratically to provide the systematic uncertainties.

Measuring cosmological parameters with a high degree of accuracy requires minimizing uncertainties of the two components of the SNIa Hubble diagram: the distance modulus and the redshift. Collecting a large sample of well-measured SNe Ia leading to accurate distance measurements is a guiding thread of this paper. It is achievable by optimizing the cadence of the survey, by adapting the number of visits per observing night, and by imposing selection criteria on photometric light curves. Redshifts can be derived either from the host galaxy (spectrum and/or photometric measurements) or from the spectrum of the SN itself. Only host galaxy spectroscopic redshifts are considered in this study. We assume that 4MOST/TiDES will provide ~ 2500 host galaxy redshifts (after 5 yr) for the DDFs (CDF-S, ELAIS-S1, and Euclid/Roman). This number of 2500 corresponds to $\sim 5\%$ of the host galaxy redshifts measured by 4MOST/TiDES (the actual number is not known yet). Equatorial fields will benefit from PFS/Subaru measurements ($\sim 20,000$ spectra after 10 yr). The current PFS/Subaru strategy is to cover 5 deg 2 (four PFS FOVs) for equatorial fields to accumulate $\sim 12,000$ host galaxy spectroscopic redshifts over 10 yr. The remaining DD area would be observed once LSST is completed. The fraction of SNe Ia expected to have secure redshift measurements is taken from Figure 1 of Mandelbaum et al. (2019).

We choose a large set of surveys among the possible configurations presented above (the observing strategy parameters are listed in Table 6):

1. DU: Five DDFs—COSMOS, XMM-LSS, CDF-S, ELAIS-S1, and Euclid/Roman—are observed every season with $z_{\text{complete}} \in [0.60, 0.80]$ ($\Delta z = 0.05$).
2. DR 10 yr: Five DDFs—COSMOS, XMM-LSS, CDF-S, ELAIS-S1, and Euclid/Roman—are observed for two seasons each according to the timeline defined in Figure 10. The redshift completeness ranges are [0.60, 0.80] and [0.50, 0.75] ($\Delta z = 0.05$) for ultradeep and deep fields, respectively.
3. IDR: Three DDFs are considered: two ultradeep fields (COSMOS and XMM-LSS) with $z_{\text{complete}} \in [0.70, 0.75, 0.80]$ and one deep field (Euclid/Roman) with $z_{\text{complete}} \in [0.50, 0.70]$ ($\Delta z = 0.05$). The ultradeep fields are observed every year and Euclid/Roman during four seasons.

The time budget as a function of the total number of well-measured SNe Ia and as a function of time is presented in Figure 12. As expected a larger number of SNe Ia are provided by the DU surveys and a minimal number by the IDR surveys with a ratio $N_{SN}^{\text{DU}} / N_{SN}^{\text{IDR},0.80} \simeq 1.8$. The shortest-time survey is obtained for IDR with a high z_{complete} (0.8) for ultradeep fields: the 5% budget limit is reached after ~ 2.6 yr.

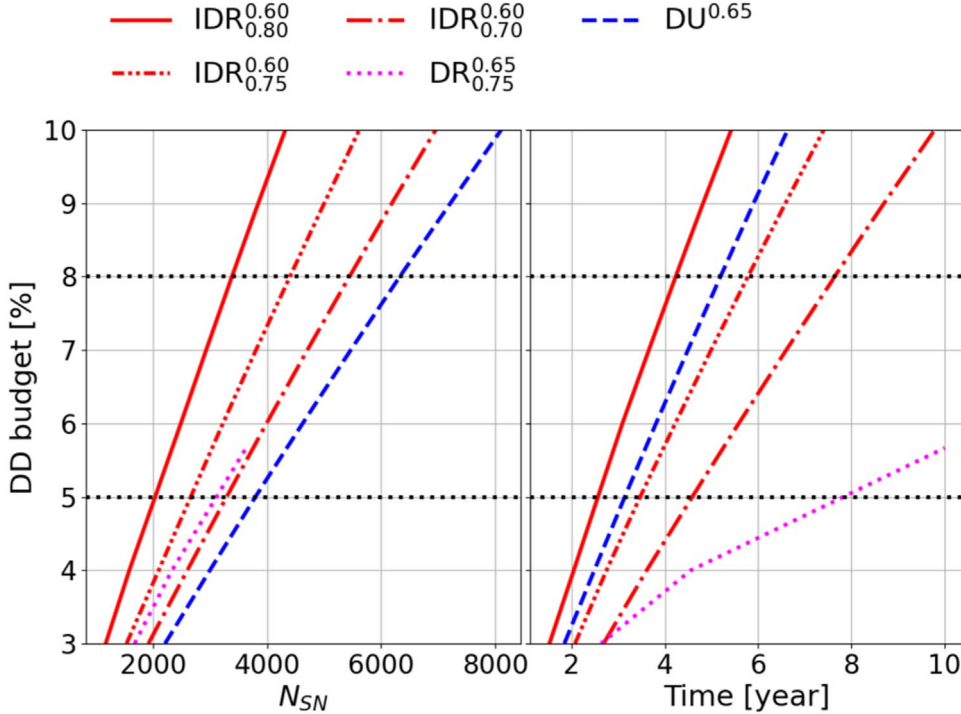


Figure 12. DD time budget as a function of the total number of well-measured SNe Ia (left) and of the time budget (right) for a set of IDR, DR, and DU surveys. Subscripts (superscripts) correspond to the redshift completeness of ultradeep (deep) fields. Black dotted lines correspond to DD time budgets of 5% and 8%.

Table 6
Observing Strategy Parameters for a Representative Set of Optimized Surveys

Observing Strategy					
Type	Name	Fields	z_{complete}	$N_{\text{seasons}}/\text{Field}$	N_{visits}
DU	DU ^{0.65}	COSMOS, XMM-LSS, ELAIS-S1, CDF-S, Euclid/Roman	0.65	10	$g/r/i/z/y$ 2/9/10/15/3
DR	DR _{0.75} ^{0.65}	COSMOS, XMM-LSS ELAIS-S1, CDF-S, Euclid/Roman	0.75 0.65	2 10	$2/9/26/35/16$ 2/9/10/15/3
IDR	IDR _{0.70} ^{0.60}	COSMOS, XMM-LSS Euclid/Roman	0.70 0.60	≥ 2 4	$2/9/20/29/7$ $2/9/1/1/0$
	IDR _{0.75} ^{0.60}	COSMOS, XMM-LSS Euclid/Roman	0.75 0.60	≥ 2 4	$2/9/26/35/16$ $2/9/1/1/0$
	IDR _{0.80} ^{0.60}	COSMOS, XMM-LSS Euclid/Roman	0.80 0.60	≥ 2 4	$2/9/37/52/21$ $2/9/1/1/0$

Note. The cadence of observation is 1 day and the season length is 180 days (maximum).

The number of well-measured SNe Ia observed in the DD survey is given in Figure 13 for the deep (CDF-S, ELAIS-S1, and Euclid/Roman) and ultradeep (COSMOS and XMM-LSS) fields. IDR surveys lead to samples mostly composed of SNe Ia observed in equatorial fields (the total number of SNe Ia provided by nonequatorial fields is ~ 100).

Since only SNe Ia with host spectroscopic redshifts are considered, the cosmological metric σ_w values depend on the spectroscopic scenario (i.e., the number of host spectroscopic redshifts per year for PFS/Subaru and 4MOST/TiDES) and on the time budget. The variation of σ_w as a function of time (years of survey) is given in Figure 14 (top left) assuming the current PFS/Subaru strategy described above. IDR surveys tend to

lead to more accurate cosmological metric estimations for the same time budget. Taking into account the whole set of spectroscopic redshifts provided by PFS/Subaru ($\sim 20,000$) leads to the results of Figure 14 (top right). Significant differences are observed between IDR and DU scenarios and a relative decrease in σ_w of about 30% for a time budget of 5% can be observed.

Measuring cosmological parameters with a high degree of accuracy with SNe requires observing a large sample of well-measured SNe Ia in the full redshift range [0.01, 1.1]. The results of Figure 14 (top) indicate that the shape of the $N_{SN}(z)$ distribution is critical to achieving low σ_w values. The profile of $N_{SN}(z)$ is affected by the Malmquist bias for $z \geq z_{\text{complete}}$ and

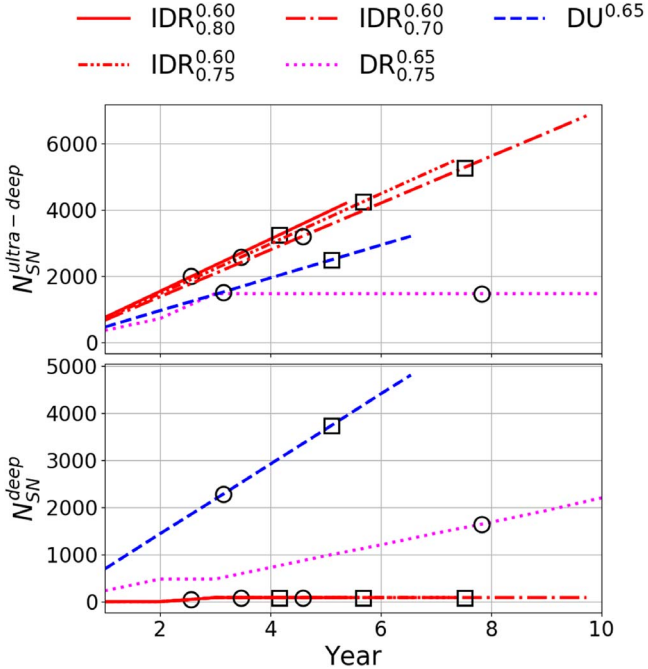


Figure 13. Number of well-measured SNe Ia observed in the DD survey as a function of time (years of survey) for deep fields (CDF-S, ELAIS-S1, and Euclid/Roman) (bottom) and ultradeep fields (COSMOS and XMM-LSS) (top). The black circles (squares) correspond to a time budget of 5% (8%).

the fraction of well-measured SNe Ia at high redshift depends on the detection threshold z_{complete} (Figure 11). Between two surveys collecting the same number of well-measured SNe Ia, the most accurate cosmological measurements are achieved by surveys characterized by the highest z_{complete} (Figure 14, top right). Low- z_{complete} surveys have to collect a higher number of well-measured SNe Ia to achieve the same accuracy.

For each of the scenarios considered in this section we estimate the FoM defined by the DETF (Albrecht et al. 2006):

$$\text{DETF FoM} = \frac{\pi}{A} \quad (16)$$

where A is the area of the confidence ellipse defined by

$$A = \pi \Delta \chi^2 \sigma_{w_0} \sigma_{w_a} \sqrt{1 - \rho^2} \quad (17)$$

with $\Delta \chi^2 = 6.17$ (95.4% confidence level). The variable ρ is the correlation factor equal to $\text{Cov}(w_0, w_a) / (\sigma_{w_0} \sigma_{w_a})$. The variables w_0 and w_a are the parameters of the Chevallier-Polarski-Linder model of the dark energy equation of state (Chevallier & Polarski 2001; Linder 2003):

$$w = w_0 + w_a \frac{z}{1+z}. \quad (18)$$

The cosmological parameters (Ω_m , w_0 , and w_a) are estimated from the minimization of Equation (15) (modified to account for the definition of w in Equation (18)) and a prior is added on the Ω_m parameter (with $\sigma_{\Omega_m} = 0.0073$; Aghanim et al. 2020).

The 2σ FoMs of the scenarios considered in this section are given in Figure 14 (bottom left and right). The conclusion is the same as above: IDR surveys lead to the highest FoM in comparison with DU surveys (+25% between IDR_{0.80} and DU^{0.65} for a DD time budget of 5%). This result reflects the abovementioned dependence of the shape of $N_{\text{SN}}(z)$ on the redshift completeness of the survey.

One of the main conclusions of the studies presented in this section is that the design of an optimal LSST DD minisurvey for cosmology with SNe Ia has to include external critical data sets such as precise host redshift measurements to be realistic. Further studies are needed to assess the impact of spectroscopic data sets from PFS/Subaru and 4MOST/TiDES, and of synergy with Euclid and the Roman Space Telescope, on the scenarios proposed in this paper. Optimizing the use of limited spectroscopic resources requires selecting DD surveys that deliver a sample containing a low number of well-measured SNe Ia while yielding accurate cosmological measurements. IDR (high- z_{complete}) surveys fulfill both criteria.

The large number of surveys presented in this section are achieved with optimal observing conditions (regular cadence and median 5σ depth). Additional simulations are required to assess the effects of realistic observing conditions such as variations of 5σ depth values or of the Moon’s brightness. Such studies might require tuning the parameters of the surveys proposed in this paper.

9. Gap/Time Budget Recovery

All the results presented above assume a regular cadence with median observing conditions (i.e., median m_5) and no translational dithering. But it is known that LSST will be affected by gaps originating from telescope downtimes related to maintenance periods and to poor observing conditions (clouds). The probability of having small gaps (estimated from the sliding windows of 180 days of the LSST baseline simulation baseline_nexp1_v1.7_10yrs) of a few nights is high (more than 80% for gaps shorter than 3 nights) and mainly due to dome closed periods (Figure 15). Larger gaps are explained by telescope maintenance times and are not exceptional: the probability of having a gap of 14 nights is about 25%. It has been shown (Section 5) that gaps affect the redshift completeness and the total number of well-measured SNe Ia, but also the DD time budget if the season length is fixed.

The metrics used up to this point have been estimated using the whole set of data. The impact of the gaps is estimated at the end of the survey. The real-time impact of the gaps on the sample of well-measured SNe Ia can be measured by a metric tracing gap effects on a nightly basis. We propose as a gap tracker metric for a night MJD_{night} the z -band S/N (S/N^z) of the median SN Ia (i.e., with $(x_1, c) = (0.0, 0.0)$) with a peak date MJD_{peak} and a redshift $z \sim 0.6$. S/N^z is estimated from the rising part of the SN Ia light curve. The value of S/N^z is constant for regular cadences (Figure 16(a)) and decreases with gaps (Figure 16(b)).

A survey with the gap distribution of Figure 16(b) leads to a decrease in z_{complete} of about 0.03 and to a loss of about 18% of well-measured SNe Ia. The time budget is also affected (-25%). Three recovery methods can be used to get $(z_{\text{complete}}, N_{\text{SN}}$, time budget) values close to those of a survey with a regular cadence (as in Figure 16(a)). The first approach would consist in recovering the initial time budget (i.e., the total number of observing nights) by adding, at the end of each season, the number of observing nights corresponding to the number of downtime nights. This method has limited effects on z_{complete} but leads to an increase of the size of the well-measured SN Ia sample due to the increase of the season length (Table 7). The second approach relies on the comparison, at the beginning of a night, between the number of visits N_{obs} and the number of expected visits N_{exp} corresponding to a survey

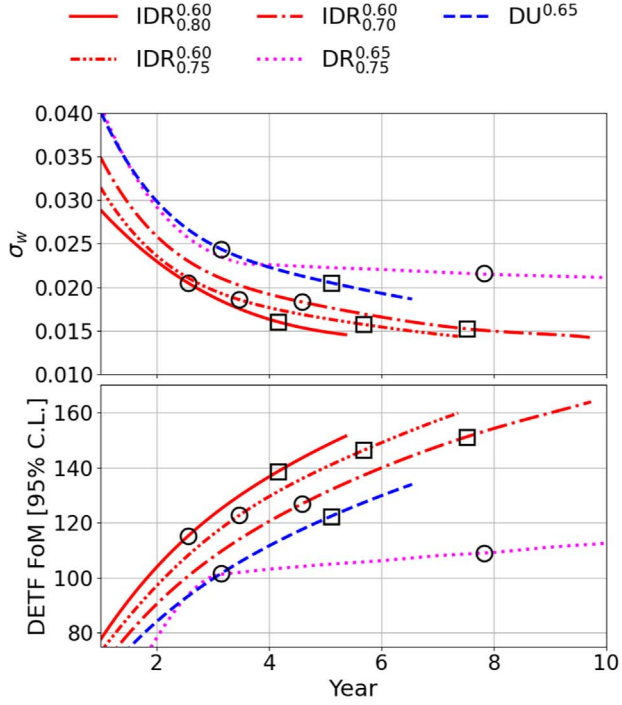


Figure 14. Left: σ_w (top) and Dark Energy Task Force (DETF) figure of merit (FoM) (bottom) as a function of time (years of survey) for scenarios with a DD time budget lower than 10%. The black circles (squares) correspond to a time budget of 5% (8%). Right: σ_w (top) and DETF FoM (bottom) after 10 yr for DD strategies considered in this paper for DD time budgets of 5% (solid line) and 8% (dashed line).

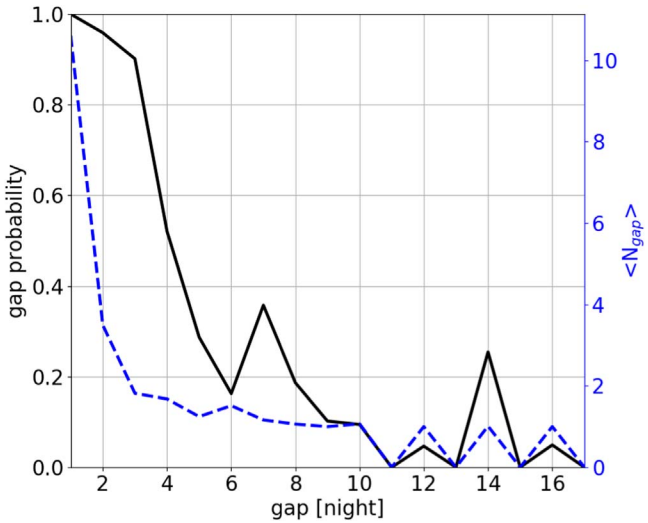
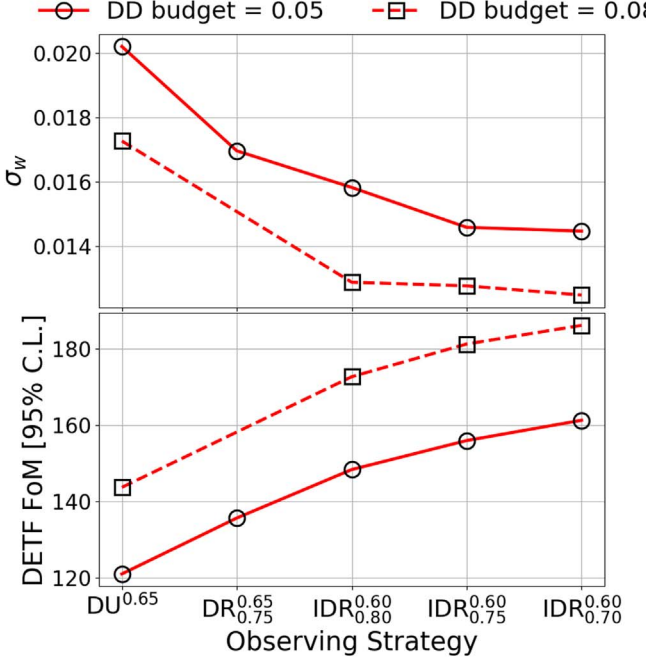


Figure 15. Probability of having gaps (full line, left y-axis) and mean number of gaps (dashed line, right y-axis) as a function of the night gap estimated with a sliding window of 180 days using the LSST baseline simulation dubbed baseline_nexp1_v1.7_10yrs.

without gaps. Observations are added while $\Delta N_{\text{visits}} = N_{\text{obs}} - N_{\text{exp}} < 0$ (Figure 16(c)). This method leads to a complete recovery of the time budget and to a minimal loss of well-measured SNe Ia (Table 7). The last approach exploits the fact that the gap tracker metric strongly decreases with gap widths. The recovery is made by adding observations if S/N^z values are lower than a threshold defined from the survey without gaps (Figure 16(a)). A partial recovery can be obtained from this method (Figure 16(d) and Table 7), which requires some tuning of the threshold value.



A closer look at the results of Table 7 indicates that one of the best ways to recover from gap effects is to extend the season length of observations. This method, however, is not applicable to all the DDFs considered in this paper. Because of their northernmost positions, COSMOS and XMM-LSS have the shortest season lengths (Figure 3) and extensions may not be possible (depending on the number of visits). In that case the second (ΔN_{visits} comparison) or third method (gap tracker) is preferred.

10. Conclusions

In this paper we have presented a three-phase study to assess the impact of the LSST DD minisurvey on the size and depth of a sample of well-measured SNe Ia: (a) thorough analysis of the DD strategy proposed by LSST, (b) development of a method to probe higher redshift completeness domains, and (c) proposal of a set of optimized DD surveys.

1. A comprehensive analysis of LSST simulations has been achieved on a subset of representative DD surveys. We have studied the impact of cadence, gaps, and translational dithering using the metric ($z_{\text{complete}}, N_{\text{SN}}$). It was shown that reaching a redshift completeness higher than 0.55–0.65 is difficult with a reasonable (~5%) time budget allocation.
2. Reaching higher redshift completeness requires increasing the S/N of the photometric light curves, while considering the redshift-dependent measured SN Ia flux per filter, cadence, and set of observing conditions. We have proposed a method providing the relationship between the optimized number of visits *per band* and the redshift completeness. We have used this result to design a set of realistic strategies.

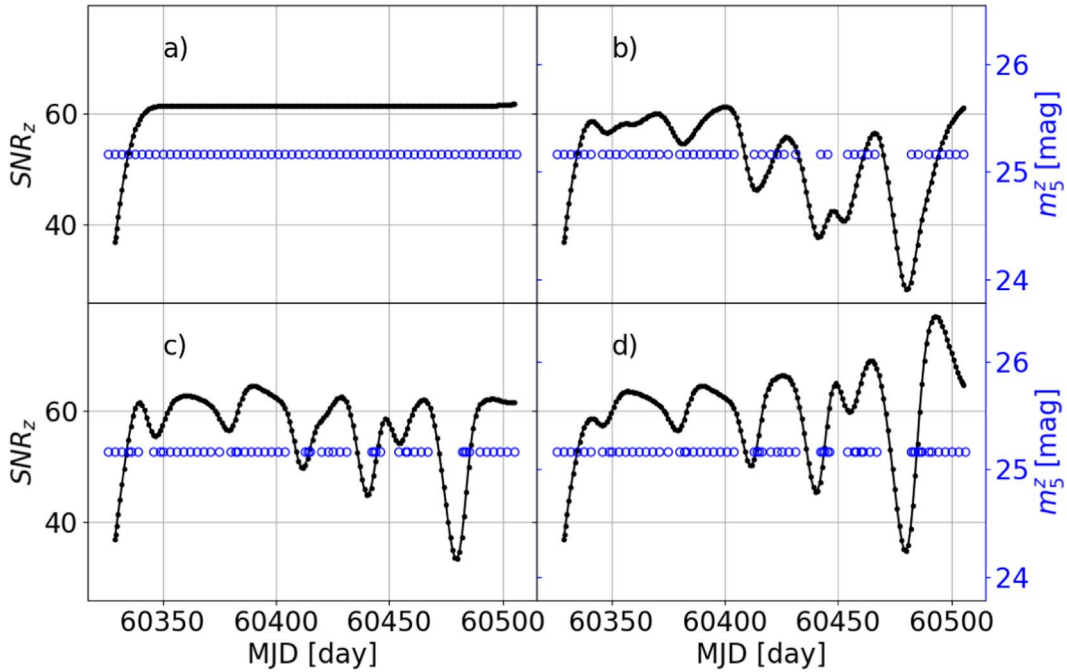


Figure 16. Gap tracker metric as a function of MJD. The full black lines correspond to S/N_z and the blue points to observations (m_5^z). Four cases are represented: 3 day cadence surveys with no gaps (a), with gaps (b), with gaps and a recovery method based on the number of visits (c), and with gaps and a recovery method based on the gap tracker metric (d).

Table 7
Variations of Time Budget, z_{complete} , N_{SN} , and Season Length (sl) for a Set of Surveys with Gaps and Three Recovery Methods

Survey	ΔBudget (%)	$\Delta z_{\text{complete}}$	ΔN_{SN} (%)	Δsl (days)
gaps	-25	-0.03	-18	0
season length extens.	0	-0.02	+11	+45
nightly ΔN_{visits}	0	-0.01	-6	0
gap tracker thresh.	-8	-0.02	-9	0

Note. The reference values are taken from a survey with a regular cadence of 3 days (no gaps) and a 6 month season length.

3. Two classes of optimized surveys have been studied. In the DU strategy all the DDFs are observed with the same cadence of observation, season length, and number of visits per observing night (i.e., the same z_{complete}). The DR strategy, where two classes of fields are defined (deep and ultradeep), aims at probing higher- z_{complete} domains. Host galaxy spectroscopic measurements from surveys contemporaneous with LSST have been included to design realistic optimized surveys.

The results shown in this paper represent a first step toward the design of an optimal LSST DD survey for cosmology with SNe Ia. Simulations of the DD survey with the LSST scheduler would help in quantifying the impact of realistic observing conditions (cadence, gaps, 5σ depth, and Moon brightness) on the proposed surveys. Additional studies are required to fully benefit from spectroscopic resources (DESI, PFS/Subaru, and 4MOST/TiDES) and to optimize the synergy with Euclid and the Roman Space Telescope.

The studies presented in this paper lead to the following main conclusions:

1. *Simulated LSST surveys do not lead to precision cosmology.* The DD surveys proposed by LSST lead to a sample of well-measured SNe Ia too shallow for measuring cosmological parameters with a high degree of accuracy. The redshift completeness of the survey is too low. Large internight gaps lead to low cadences of observation and to a dramatic decrease in the SN Ia sample size (up to 30%). Having a deterministic scheduler would provide significant improvements in the quality of the survey, in terms of cadence regularity or season length. The scheduler could include metrics (gap recovery mechanisms) to monitor the DD survey on a nightly basis and to correct for gaps so as to achieve a high-quality observing strategy for SN Ia cosmology with LSST. Large translational dithers reduce the DDF area observed with high cadence and lead to a dramatic decrease of the number of well-measured SNe Ia for low-cadence surveys.

2. *IDR is preferred for precision cosmology.* Of the variety of optimized DD surveys studied in this paper, IDR surveys lead to the most accurate cosmological measurements. They are characterized by a minimal configuration of three fields—two ultradeep (COSMOS and XMM-LSS up to $z_{\text{complete}} \sim 0.8$) and one deep (Euclid/Roman up to $z_{\text{complete}} \sim 0.6$). These scenarios require a high cadence of observation (every night) and a large number of visits per night and per field (about 130 visits per single ultradeep field) and could be achieved in just a few years.

Measuring cosmological parameters with a high degree of accuracy requires having a sample of well-measured SNe Ia with a significant fraction of SNe at higher redshifts. This fraction increases with the redshift

completeness of the sample. IDR surveys are characterized by the highest z_{complete} and lead to the best FoM.

3. *Accurate z_{host} is critical for precision cosmology.* The accuracy of cosmological measurements with SNe Ia is crucially dependent on the precision of the host galaxy redshifts (x -axis of the Hubble diagram). We have chosen, in this paper, to optimize DD surveys with the assumption that host galaxy spectroscopic redshifts are available for almost all of the well-measured SNe Ia used to perform cosmological measurements.

Spectroscopic resources will be critical for higher-redshift ($z \gtrsim 0.7$) SNe Ia that significantly contribute to the measurement of cosmological parameters such as (w_0, w_a) . PFS/Subaru is currently the only survey able to provide a significant number of spectra (a few thousands) in the range $z \in [0.7, 1.1]$ during the LSST era. This explains why the best strategies proposed in this paper are based on the intense observation of two equatorial fields (COSMOS and XMM-LSS). Only half of the well-measured SN Ia sample benefit from host galaxy spectroscopic measurements with the current PFS/Subaru strategy. Final cosmological measurements within 3 yr of a survey with the full SN Ia sample would involve the delivery of about 800 spectroscopic redshifts by PFS/Subaru per year with eight PFS FOVs per equatorial field.

Additional studies are required for the southern fields, which benefit from 4MOST/TiDES host galaxy spectroscopic redshift measurements. The performance of optimized strategies has been obtained under the assumption that the fraction of SNe Ia expected to have secure measurements in the deep fields is identical for WFD fields and DDFs (this fraction is not known for DDFs yet). This is probably pessimistic for DDFs and this fraction will probably be higher at high z (it is $\sim 20\%$ for $z = 0.7$ for WFD fields). The accuracy of cosmological measurements would improve with an increase of the fraction of SNe Ia with secure measurements of higher redshifts.

4. Photometric redshifts, number of fields, and time budget.

Using photometric redshifts to perform accurate cosmological measurements with SNe Ia in a Hubble diagram is a challenging task. It requires measuring photo- z with a high degree of accuracy and controlling catastrophic outlier redshifts to minimize photo- z systematics. The current LSST minimal target $\sigma_z \sim 0.02(1 + z_{\text{phot}})$ (Graham et al. 2018) induces an error on the distance modulus higher than 0.10 mag (full redshift range). A lot of effort is being made to develop techniques leading to lower σ_z (Schmidt et al. 2020). But it will be difficult to reach an accuracy similar to that of spectroscopic measurements ($\sigma_z \sim 10^{-3}$) and to have a set of photo- z with a precision corresponding to the stringent calibration requirements of LSST (The LSST Dark Energy Science Collaboration et al. 2018).

Cosmological measurements from SN surveys have historically been achieved with host galaxy spectroscopic redshift measurements (see, e.g., Scolnic et al. 2018a; Abbott et al. 2019; Brout et al. 2022). A recent study (Chen et al. 2022) has shown the feasibility of performing SN cosmology using photo- z . Using a set of 125 photometrically classified SNe Ia located in luminous red galaxies with photo- z accuracy similar to the LSST

minimal target, a difference in Δw versus spectroscopic redshifts of about 0.005 was found in data and a difference of 0.01–0.02 was found in simulations. While these results are encouraging, further work is probably needed to achieve the same accuracy in the general population of galaxies.

It is possible to estimate the fraction of SNe Ia with photo- z in the optimal DD surveys studied in this paper. If 8% of LSST time is spent on DDFs, the results for two representative scenarios are as follows:

- (a) IDR_{0.60}^{0.70} survey: Less than 5500 well-measured SNe Ia are expected to be observed from the ultradeep fields and less than 100 from the deep fields. According to the expected number of spectroscopic galaxy redshift measurements by PFS/Subaru and 4MOST/TiDES, we end up with about 20 SNe Ia (0.3%) with photometric redshifts (in deep fields).
- (b) In the scenario where all the DDFs that the VRO guarantees to observe are included, it would be reasonable to opt for surveys optimizing the use of spectroscopic resources to guarantee a minimal FoM that could be improved by complementary surveys with sets of SNe Ia with photo- z . The survey could be composed of an IDR_{0.80}^{0.60} strategy using $\sim 5\%$ of the DD time budget (in ~ 3 yr) followed by a DU^{0.65} survey with the remaining four fields observed for two seasons each. A total of 2000 well-measured SNe Ia are expected to be observed in the ultradeep fields, all of them with a host galaxy spectroscopic redshift measured by PFS/Subaru. A total of 1430 well-measured SNe Ia are expected to be observed in the deep fields, out of which 559 (16% of the total number of well-measured SNe Ia) have photo- z measured by 4MOST/TiDES. In this scenario, a minimal DETF FoM of 150 would be guaranteed and all the DDFs would be observed.

The DESC acknowledges ongoing support from the Institut National de Physique Nucléaire et de Physique des Particules in France; the Science & Technology Facilities Council in the United Kingdom; and the Department of Energy, the National Science Foundation, and the LSST Corporation in the United States. DESC uses resources of the IN2P3 Computing Center (CC-IN2P3–Lyon/Villeurbanne—France) funded by the Centre National de la Recherche Scientifique; the National Energy Research Scientific Computing Center, a DOE Office of Science User Facility supported by the Office of Science of the U.S. Department of Energy under Contract No. DE-AC02-05CH11231; STFC DiRAC HPC Facilities, funded by UK BIS National E-infrastructure capital grants; and the UK particle physics grid, supported by the GridPP Collaboration. This work was performed in part under DOE Contract DE-AC02-76SF00515. M.L. acknowledges support from the South African Radio Astronomy Observatory and the National Research Foundation (NRF) toward this research. Opinions expressed and conclusions arrived at are those of the authors and are not necessarily to be attributed to the NRF. H.A. acknowledges support from a Leinweber Postdoctoral Research Fellowship and DOE grant DE-SC009193. I.H. acknowledges support from the Science and Technologies Facilities Council

grant No. ST/V000713/1. This paper has undergone internal review in the LSST Dark Energy Science Collaboration.

This research has made use of the following Python software packages: NumPy (van der Walt et al. 2011), SciPy (Virtanen et al. 2020), Matplotlib (Hunter et al. 2007), Astropy (Price-Whelan et al. 2018), SNCosmo (Barbary et al. 2016), and Pandas (McKinney 2011).

Author contributions are as follows. Philippe Gris: conceptualization, software, analysis, and writing. Nicolas Regnault: conceptualization, analysis, and writing. Humna Awan: participated in (and led some) discussions on DD survey optimization, especially in regard to the translational (and rotational) dithering of observations; provided detailed comments on the paper during collaboration review, which hopefully strengthened the paper and made its key takeaways clearer; and contributed to the general optimization of survey sims via builder work. Isobel Hook: general paper discussion/suggestions; acted as internal reviewer, whose comments led to several improvements, e.g., clarification of the underlying metric of success used in this paper (Section 7). Saurabh Jha: builder; enabling contributions included helping to develop the emphasis on “well-measured” SNe in Section 2.1 and Section 4 (per-object uncertainty less than or on the order of the SN Ia intrinsic scatter); suggested some of the survey strategies considered in Table 3; participated in (and led some) discussions of paper content and helped oversee paper review as Observing Strategy Working Group co-convener. Michelle Lochner: general paper discussion/suggestions including y -band optimization analysis and FoM implementation; edits of the draft; co-lead of the Observing Strategy Working Group, which provided context for strategies proposed in this paper, particularly the rolling strategies; builder. Bruno Sanchez: general discussions; SNWG co-convener. Dan Scolnic: general paper discussion/suggestions; acted as internal reviewer, with comments on earlier sections and the framing of the metrics used; co-led Observing Strategy Working Group, which provided context for strategies proposed in this paper, particularly the rolling strategies. Mark Sullivan: general paper discussion/suggestions; internal reviewer during review process, providing significant/detailed comments that led to several changes in the paper. Peter Yoachim: observing strategy simulations.

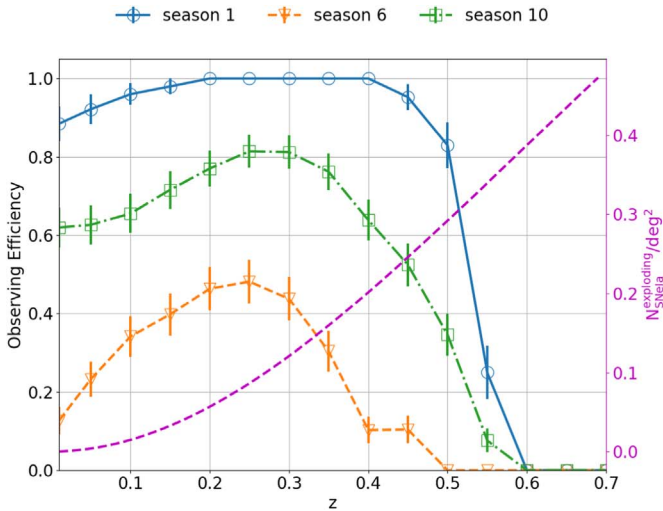


Figure A1. Left: Observing efficiencies (color curves) and number of exploding SNe Ia per square degree (purple dashed curve) as a function of the redshift. Right: Normalized cumulative distribution of the number of well-measured faint SNe as a function of redshift. The 95th percentile limit defines the z_{complete} value. These plots correspond to one HEALPix pixel of the CDF-S field (with the number 144428) of the daily strategy.

Appendix A Metric ($N_{\text{SN}}^{z \leq z_{\text{complete}}}$, z_{complete}) Estimation

The pair metric ($N_{\text{SN}}^{z \leq z_{\text{complete}}}$, z_{complete}) is estimated from the combination of observing efficiency curves and SN Ia production rates. Observing efficiencies are estimated from a set of simulated light curves of SNe Ia. A systematic scan of the SN Ia parameter space (T_0, z) is performed for SNe Ia with $(x_1, c) = (-2.0, 0.2)$ and $(x_1, c) = (0.0, 0.0)$ to estimate efficiency curves with a high degree of accuracy: $z \in [0.01, 1.0]$ (step: 0.05) and $T_0 \in [\text{MJD}_{\text{season}}^{\text{min}} + 15 * (1+z), \text{MJD}_{\text{season}}^{\text{max}} - 30 * (1+z)]$ (step: 2 days), where MJD is the modified Julian date. The observing efficiency is defined as the fraction of simulated light curves fulfilling the requirements defined in Section 4, per redshift bin. Example curves are given in Figure A1 (left). For a regular cadence, one would expect to have the following (reference) shape: flat efficiency (close to 1) up to a completeness redshift beyond which efficiency decreases down to 0. Figure A1 (left) reveals that, in practice, efficiency curves may significantly deviate from this reference shape: while results achieved in season 1 are satisfactory, it appears that observations collected in season 6 lead to poor efficiency curves (less than 50% at maximum). This difference is primarily explained by the cadence of observation and the internight gaps that drive the sampling frequency of the light-curve measurements.

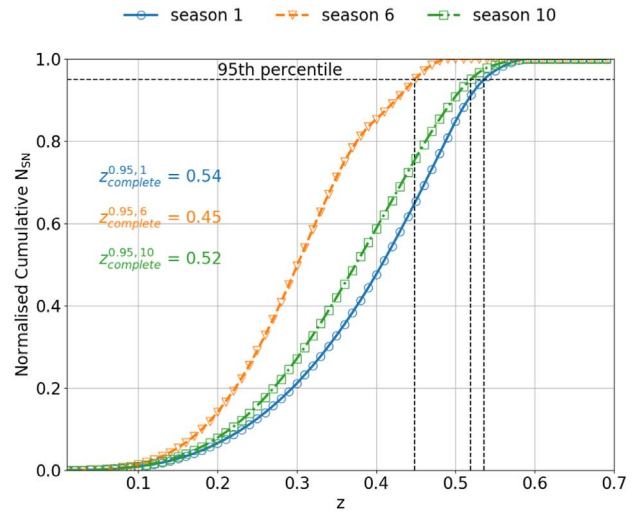
The number of well-measured SNe Ia is estimated from the combination of efficiency curves and a number of exploding SNe Ia per square degree:

$$N_{\text{SN}}(z) = \text{efficiency}(z) \times N_{\text{SNe Ia}}^{\text{exploding}}(z)/\text{deg}^2 \times \text{area} \quad (19)$$

where area is the observed area (a HEALPix pixel area) and

$$N_{\text{SNe Ia}}^{\text{exploding}}(z)/\text{deg}^2 = \text{Rate}_{\text{SNe Ia}} \times V \quad (20)$$

where $\text{Rate}_{\text{SNe Ia}}$ is the volumetric SN Ia rate and V is the comoving volume (Perrett et al. 2012). The normalized cumulative sum of N_{SN} is used to estimate the redshift completeness as illustrated in Figure A1 (right). The results are then used as input to estimate the number of well-sampled SNe Ia up to $z \leq z_{\text{complete}}$, $N_{\text{SN}}^{z \leq z_{\text{complete}}}$.



Appendix B

Impact of the SALT3 Model on z_{complete} Estimation

We estimate the z_{complete} values for SALT3 and SALT2 models using the same observing strategy parameters (cadence of 1 day and number of visits per band and per observing night taken from Figure 8) and similar observing conditions ($m_5(\text{single exposure}) = 24.49, 24.04, 23.6, 22.98, 22.14$ for the g, r, i, z, y bands, respectively). The results (Figure B1)

show a slight improvement for the SALT3 model: for $z \gtrsim 0.7$, only the izy bands are used and the z_{complete} values are systematically higher for the SALT3 model and the difference with SALT2 tends to increase with z_{complete} but does not exceed ~ 0.03 at higher z_{complete} . This slight improvement is explained by the extended wavelength range 2000–11000 Å (1800 Å redder) and reduced uncertainties of the SALT3 model as compared to SALT2 (Kenworthy et al. 2021).

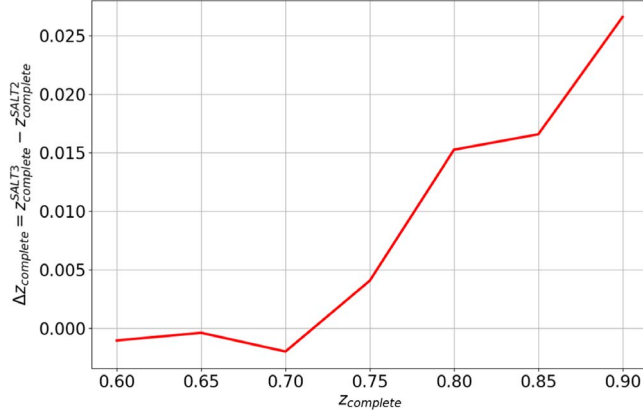


Figure B1. z_{complete} difference between estimations of the SALT3 and SALT2 models as a function of z_{complete} estimated using the SALT2 model.

Appendix C Realistic Simulations Using σ_μ and N_{SN}

The method used to estimate cosmological parameters (Section 6) relies on the simulation of distance moduli and requires knowledge of σ_μ and N_{SN} as a function of z . These two quantities are estimated from a full simulation and fit of

SN Ia light curves. The simulations are performed for a set of redshift completeness values, namely $z_{\text{complete}} \in [0.50, 0.90]$ (step: 0.05), so as to include Malmquist bias effects as illustrated by Figure C1: the dependence of σ_μ on z_{complete} and the decrease of N_{SN} for $z \geq z_{\text{complete}}$ are to be explained by the redshift bias.

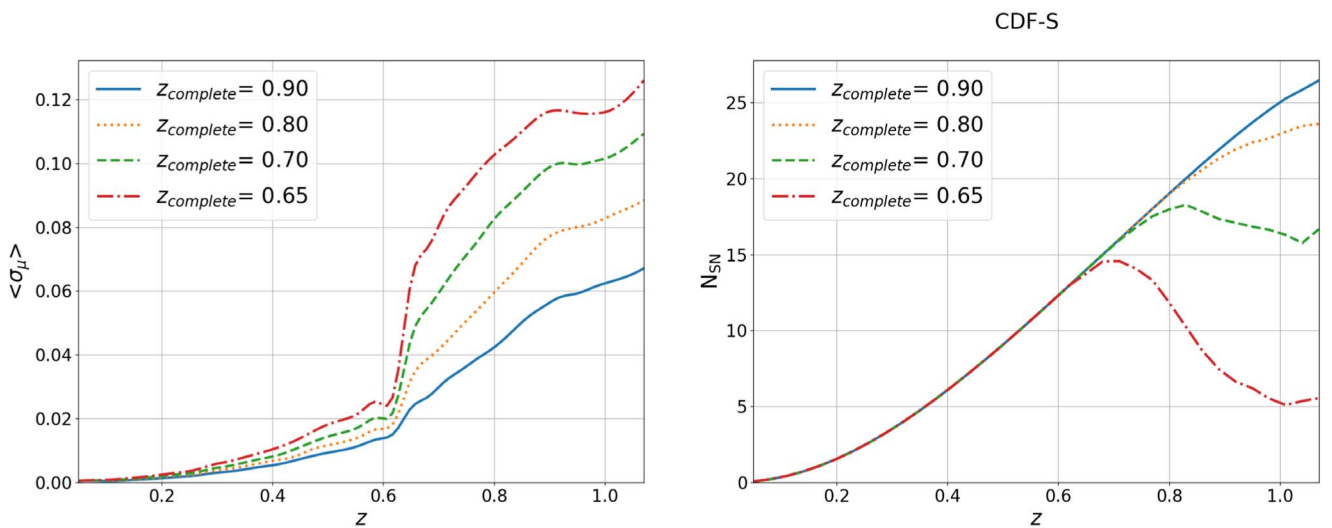


Figure C1. Left: Mean values of σ_μ as a function of the redshift for a set of surveys labeled by the redshift completeness. Right: Number of SNe Ia as a function of the redshift for a set of surveys labeled by the redshift completeness for the CDF-S field (survey area of 9.6 deg^2 and season length of 180 days).

ORCID iDs

- Philippe Gris <https://orcid.org/0000-0001-5673-0959>
 Nicolas Regnault <https://orcid.org/0000-0001-7029-7901>
 Humna Awan <https://orcid.org/0000-0003-2296-7717>
 Isobel Hook <https://orcid.org/0000-0002-2960-978X>
 Saurabh W. Jha <https://orcid.org/0000-0001-8738-6011>
 Michelle Lochner <https://orcid.org/0000-0003-2221-8281>
 Bruno Sanchez <https://orcid.org/0000-0002-8687-0669>
 Mark Sullivan <https://orcid.org/0000-0001-9053-4820>
 Peter Yoachim <https://orcid.org/0000-0003-2874-6464>

References

- Abbott, T. M. C., Allam, S., Andersen, P., et al. 2019, *ApJL*, **872**, L30
 Aghanim, N., Akrami, Y., Ashdown, M., et al. 2020, *A&A*, **641**, A6
 Albrecht, A., Bernstein, G., Cahn, R., et al. 2006, arXiv:[astro-ph/0609591](#)
 Amendola, L., Appleby, S., Bacon, D., et al. 2013, *LRR*, **16**, 6
 Awan, H., Gawiser, E., Kurczynski, P., et al. 2016, *ApJ*, **829**, 50
 Barbary, K., Barclay, T., Biswas, R., et al. 2016, SNCosmo: Python library for supernova cosmology Astrophysics Source Code Library, [ascl:1611.017](#)
 Betoule, M., Kessler, R., Guy, J., et al. 2014, *A&A*, **568**, A22
 Bianco, F. B., Ivezić, Ž., Jones, R. L., et al. 2021, *ApJS*, **258**, 1
 Brout, D., & Scolnic, D. 2021, *ApJ*, **909**, 26
 Brout, D., Scolnic, D., Kessler, R., et al. 2019, *ApJ*, **874**, 150
 Brout, D., Scolnic, D., Popovic, B., et al. 2022, *ApJ*, **938**, 110
 Burke, D. L., Rykoff, E. S., Allam, S., et al. 2017, *AJ*, **155**, 41
 Chen, R., Scolnic, D., Rozo, E., et al. 2022, *ApJ*, **938**, 62
 Chevallier, M., & Polarski, D. 2001, *JMPD*, **10**, 213
 DESI Collaboration, Aghamousa, A., Aguilar, J., Ahlen, S., et al. 2016, arXiv:[1611.00036](#)
 de Jong, R., Agertz, O., Berbel, A. A., et al. 2019, *Msngr*, **175**, 3
 Gorski, K. M., Hivon, E., Banday, A. J., et al. 2005, *ApJ*, **622**, 759
 Graham, M. L., Connolly, A. J., Ivezić, V., et al. 2018, *AJ*, **155**, 1
 Guy, J., Astier, P., Baumont, S., et al. 2007, *A&A*, **466**, 11
 Guy, J., Sullivan, M., Conley, A., et al. 2010, *A&A*, **523**, A7
 High, F. W., Stubbs, C. W., Stalder, B., Gilmore, D. K., & Tonry, J. L. 2010, *PASP*, **122**, 722
 Hunter, J. D. 2007, *CSE*, **9**, 90
 Ivezić, V., Kahn, S. M., Tyson, J. A., et al. 2019, *ApJ*, **873**, 111
 Kenworthy, W. D., Jones, D. O., Dai, M., et al. 2021, *ApJ*, **923**, 265
 Kessler, R., Guy, J., Marriner, J., et al. 2013, *ApJ*, **764**, 48
 Kessler, R., & Scolnic, D. 2017, *ApJ*, **836**, 56
 Laureijs, R., Amiaux, J., Arduini, S., et al. 2011, arXiv:[1110.3193](#)
 Linder, E. V. 2003, *PhRvL*, **90**, 091301
 Lochner, M., Scolnic, D., Almoubayyed, H., et al. 2022, *ApJS*, **259**, 58
 Lochner, M., Scolnic, D., Almoubayyed, H., et al. 2021, The LSST Dark Energy Collaboration Cadence Note, [https://docushare.lsst.org/docushare/dsweb/Get/Document-37643/DESC_Cadence_Note.pdf](#)
 LSST Science Collaboration, Abell, P. A., Allison, J., et al. 2009, arXiv:[0912.0201](#)
 Magnier, E. A., Schlaflay, E. F., Finkbeiner, D. P., et al. 2020, *ApJS*, **251**, 6
 Malmquist, K. G. 1922, *MeLuF*, **100**, 1
 Mandelbaum, R., Blazek, J., Chisari, N. E., et al. 2019, *BAAS*, **51**, 363
 McKinney, W. 2011, Proc. of the 9th Python in Science Conf., ed. S. van der Walt & J. Millman, **56**, [https://conference.scipy.org/proceedings/scipy2010/mckinney.html](#)
 Naghib, E., Yoachim, P., Vanderbei, R. J., Connolly, A. J., & Jones, R. L. 2019, *AJ*, **157**, 151
 Padmanabhan, N., Schlegel, D. J., Finkbeiner, D. P., et al. 2008, *ApJ*, **674**, 1217
 Perrett, K., Sullivan, M. A. C., Conley, A., et al. 2012, *AJ*, **144**, 59
 Price-Whelan, A. M., Sipőcz, B. M., Günther, H. M., et al. 2018, *AJ*, **156**, 123
 Regnault, N., Conley, A., Guy, J., et al. 2009, *A&A*, **506**, 999
 Riess, A. G., Casertano, S., Yuan, W., Macri, L. M., & Scolnic, D. 2019, *ApJ*, **876**, 85
 Schlaflay, E. F., Finkbeiner, D. P., Jurić, M., et al. 2012, *ApJ*, **756**, 158
 Schmidt, S. J., Malz, A. I., Soo, J. Y. H., et al. 2020, *MNRAS*, **499**, 1587
 Scolnic, D., & Kessler, R. 2016, *ApJL*, **822**, L35
 Scolnic, D. M., Jones, D. O., Rest, A., et al. 2018a, *ApJ*, **859**, 101
 Scolnic, D. M., Lochner, M., Gris, P., et al. 2018b, arXiv:[1812.00516](#)
 Spergel, D., Gehrels, N., Baltay, C., et al. 2015, arXiv:[1503.03757](#)
 Swann, E., Sullivan, M., Carrick, J., et al. 2019, *Msngr*, **175**, 58
 Tamura, N., Takato, N., Shimono, A., et al. 2016, *Proc. SPIE*, **9908**, 99081M
 Teerikorpi, P. 2015, *A&A*, **576**, A75
 The LSST Dark Energy Science Collaboration, Mandelbaum, R., Eifler, T., et al. 2018, arXiv:[1809.01669](#)
 Tripp, R., & Branch, D. 1999, *ApJ*, **525**, 209
 van der Walt, S., Colbert, S. C., & Varoquaux, G. 2011, *CSE*, **13**, 22
 Virtanen, P., Gommers, R., Oliphant, T. E., et al. 2020, *NatMe*, **17**, 261